Available online at www.sciencedirect.com
SCIENCE DIRECT
Journal of African Earth Sciences 45 (2006) 257–278
Journal of African Earth Sciences
www.elsevier.com/locate/jafrearsci

# Crustal evaluation of the northern Red Sea rift and Gulf of Suez, Egypt from geophysical data: 3-dimensional modeling

Salah Saleh [a,b], Thomas Jahr [b], Gerhard Jentzsch [b,*], Ahmed Saleh [a], N.M. Abou Ashour [c]

[a] National Research Institute of Astronomy and Geophysics, 11421 Helwan, Cairo, Egypt
[b] Institut für Geowissenschaften, Friedrich-Schiller-Universität, Burgweg 11, D-07749 Jena, Germany
[c] Ain Shams University, Faculty of Science, Geophysical Department, Cairo, Egypt

Received 8 December 2003; received in revised form 31 May 2005; accepted 6 February 2006
Available online 29 March 2006

**Abstract**

Combined 3-D interpretations of gravity and aeromagnetic data have been used in addition to continental and marine seismic profiles, well logs and geological cross-sections. The combination of gravity and magnetic data has improved the geometry and the density distribution in the 3-D calculated profiles. Results of the current work reveal possible crustal thickness and density distribution between the sedimentary cover and the upper mantle including the Moho discontinuity. The Moho depth map of the region, as obtained from the 3-D modeling exhibits various crustal thickness distributions. The type of crust changes gradually from continental to oceanic, from north to south. The zone of crustal thinning coincides mostly with zones of low-density, heated anomalous upper mantle beneath the rift floor (7 km). The eastern plateaus (the Red Sea hills) show by far the largest crustal thickness in the region (32 km).

The Moho relief, as indicated from magnetic interpretation, shows a poor flattening especially in the eastern region. This is contrary to what is given by other authors. However, the present results are in good agreement with the geothermal gradient values in the Red Sea.

The interpretation of magnetic data of the Red Sea Rift shows that the spreading rate of the part south of latitude 26.5° N agrees well with the theoretical model, in the order of 0.7 cm/yr. Less agreement has been obtained in the part north of latitude 27.5° N.

The magnetic anomalies along the axial portion of the rift floor, as deduced from the results of the regional and residual separation and the 3-D magnetic modeling, are mainly caused by the oceanic crustal structures beneath the graben.


*Keywords:* 3-Dimensional modeling; Bouguer and magnetic anomalies; Red Sea rift; Gulf of Suez; Egyptian off-shore

## 1. Introduction

The Red Sea is considered to be a typical example of a newly formed ocean; therefore, a great number of studies discuss its evolution as a key for understanding continental rifting and the initiation of sea floor spreading (Drake and Girdler, 1964; Tramontini and Davies, 1969; Makris et al., 1983; Gaulier et al., 1988; Martinez and Cochran, 1988; Cochran and Martinez, 1988; Meshref, 1990).

Drake and Girdler (1964), Tramontini and Davies (1969) indicated that the recorded seismic velocities are 5.8–5.9 km/s for the upper crust in the northern Red Sea, and the crust appears to be somewhat inhomogeneous in this area. Also, it was stated that the northern part of the Red Sea appears to be characterized by oceanic type crust, lying at a mean depth of 7–8 km, whereas the Moho is at a mean depth of 10–13 km, and at 32 km closest to the coastline (Gaulier et al., 1988; Makris et al., 1991; Rihm et al., 1991).

Data presented in Cochran and Martinez (1988) and in Martinez and Cochran (1988) imply that extension in the northern Red Sea has recently become concentrated in a

* Corresponding author. Fax: +49 3641 948662.
*E-mail address:* Gerhard.Jentzsch@uni-jena.de (G. Jentzsch).

1464-343X/$ - see front matter © 2006 Elsevier Ltd. All rights reserved.
doi:10.1016/j.jafrearsci.2006.02.001

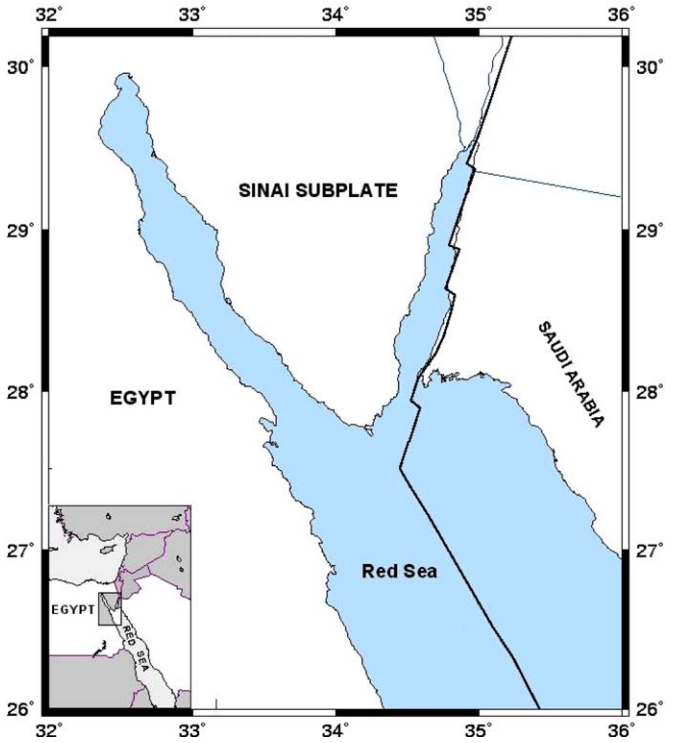


Fig. 1. Location map for the area of study.

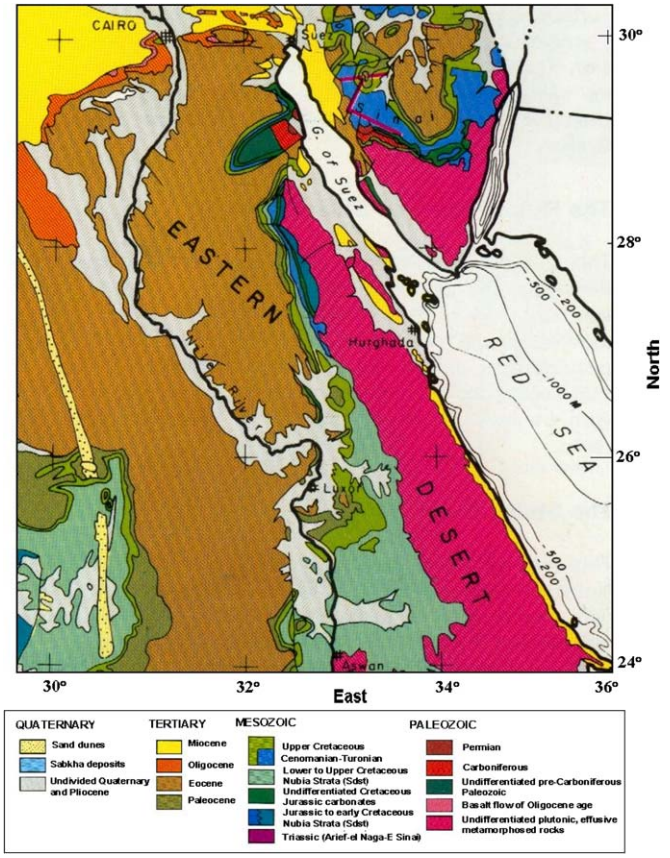


Fig. 2. Surface geological map for the region of study (from Egyptian Geological Survey, 1994).

well defined axial depression, which is considered to be a narrow plate boundary. Cochran and Martinez (1988) stated that the northern Red Sea occupies a critical position in the transition from continental to oceanic extension in a rift. Observations of its structure and tectonics allow a qualitative model for that transition to be developed.

On land, refraction data indicate a Moho depth of 35–40 km with a velocity 8.0 km/s, in the areas which are not affected by the rifting process and where the crust is found to be continental (Ginzburg et al., 1981; Makris et al., 1983; Gettings et al., 1986; El-Isa et al., 1987).

In the current study integrated geophysical methods (gravity and magnetic) have been applied to determine the sub-surface structural nature in a 3-dimensional model. All the available gravity and magnetic data (General Petroleum Corporation, 1986; Kamel, 1990), the gravity map of the Sinai Peninsula (Tealeb and Riad, 1986), the recent available marine gravity, magnetic and well logging data (Minich, 1987; Cochran et al., 1986; Martinez and Cochran, 1988; Meshref, 1990; General Petroleum Corporation, 1980) were all considered. This is used to construct a new model of the composition of the crust and its present state, continental or oceanic, especially in the areas where the transition took place (See. Fig. 1).

## 2. Geological setting

The oldest known formation in the study area is of Late Precambrian age, igneous and metamorphic rocks forming the northern edge of the African Shield (Fig. 2). The basement complex outcrops in southern Sinai and in the Eastern Desert (Red Sea mountain range).

Said (1962) and El-Gezeery and Marsouk (1974) showed that the depth of the basement increases northwards towards the Mediterranean Sea. The Palaeozoic rocks are characterized by continental clastic deposits. The marine episodes are minor in space and time. The Palaeozoic period ends with the Upper Carboniferous-Lower Permian marine deposition that followed the Hercynian orogenic phase, and the subsequent erosional period. Predominant continental deposition started again in the Mesozoic. A Middle Triassic marine transgression from the Tethys appears to be limited to the area of northern Sinai and the Gulf of Suez. Jurassic deposits cover parts of the west side of the Gulf of Suez; it appears that the distribution of the Jurassic sediments around the Gulf is as far south as Wadi Araba. The sediments include fluvio-marine and marine shallow-water deposits. The maximum extension of the sea seems to have occurred during Middle Jurassic time. The Cenozoic witnessed the transformation of the Tethys into the Mediterranean Sea. During the Palaeocene–Eocene, 'deep sea conditions' migrated southwards and shallow water conditions of sedimentation or even land masses resulted in the northern part of Egypt, which now corresponds to the southern Mediterranean Sea. The deep sea conditions in the south left thick calcareous deposits, succeeded by Eocene limestones, which are the

most widespread marine deposits in Egypt. This limestone extends over the central part of the country where it constitutes a large plateau, crossed by the River Nile over a distance of 400 miles, and in the central part of Sinai. The Miocene was a period of great transformation, leading to the present Red Sea coast sediments and similar sedimentation in the north-western part of the Gulf of Suez. After the Oligocene uplift, an Early and Middle Miocene Tethys transgression began, only to be followed by late Miocene regression related to Alpine orogeny to the north. More extensive marine beds were formed in the Miocene, with a maximum extent in the Middle Miocene, when they reached to the Gulf of Suez and the Red Sea region beyond the Egyptian border. Pliocene sediments are widely distributed along the Red Sea. The Quaternary was characterized by regression with minor transgression. Uplift and tectonic disturbances mark the Pliocene-Quaternary boundary in the Red Sea region. Volcanism occurred in the Red Sea axial trough (El-Gezeery and Marsouk, 1974).

## 3. Gravity data

A considerable amount of gravity data are now available to unravel the gross crustal structure of the Red Sea region. In the present work we utilize the following data: (1) Bouguer gravity data of the Egyptian General Petroleum Company (EGPC, 1980) which was published as a set of Bouguer maps of Egypt at 1:500,000 scale by compiling all available gravity data. A simplified and redrawn version of this map is presented. (2) Gravity surveys for the study region were conducted by the Sahara Petroleum Company (SAPETCO) and PHILIPS Company between 1954 and 1958. These surveys covered a large area of the Gulf of Suez, Sinai and the Eastern Desert. All the data of these surveys were compiled, classified and ranked according to instrument sensitivity and measurement density. The gravity measurements were conducted using two Worden gravimeters. The instruments are temperature compensated and have a sensitivity of $\pm 0.1$ mGal[1] (Kamel, 1990). (3) Marine gravity data in the northern Red Sea were taken from publications (Minich, 1987; Martinez and Cochran, 1988). The underwater gravity survey was conducted using a Bell Aerospace BGM-3 marine gravity meter system that was installed on the R/V "Robert D. Conrad", north of 26° N, in 1984. The system consisted of a vertical component forced feedback accelerometer which is not subject to cross coupling errors, mounted on a gyro-stabilized platform. The performance of this system is described in detailed by Bell and Watts (1986). In the Red Sea, gravity data values were obtained at 1 min intervals, with discrepancies at ship track intersections of less than about 1 mGal for the northern sections, and not more than about 3 mGal in the worst cases. Data from previous cruises in the area were included in our contour map if discrepancies at intersections of individual ship tracks and scatter of their discrepancies at intersections with the new data were less than 7 mGal. Those cruises satisfying the above criteria and their data, adjusted by adding a constant to remove the average gravity discrepancy at intersections with those cruises, as well as (4) Sinai Peninsula data, were collected, from Tealeb and Riad (1986).

### 3.1. Gravity data analysis

Fig. 3 shows the gravity data distribution of the study area (dots). The distance between the consecutive observation stations ranges from approximately 2–5 km. The calculated Bouguer gravity anomaly is: (1) based on the international gravity formula of 1967, referenced to the IGSN-1971, reduced to sea level and corrected with the standard density of reduction, 2670 kg/m$^3$.

For onshore stations, terrain corrections up to 50 m were made in the field using topographic charts and Hammer tables (Hammer, 1939). The horizontal positions of the stations were obtained from 1:500,000 topographic sheets. The station locations were converted to the Universal Transverse grid coordinates with the central Meridian at 30° E. Elevations at each station were measured by a barometric altimeter and all measurements are referenced to absolute elevation. The corrections were applied to all land stations. These corrections generally are $\leqslant 1$ mGal, however, along the mountains of the Red sea hills they reach more than 4 mGal.

The combined errors in the Bouguer gravity values depend upon the sum of errors in observation, elevation and terrain corrections. i.e.

$$\varepsilon_B^2 = \sqrt{(\varepsilon_g^2 + \varepsilon_h^2 + \varepsilon_p^2 + \varepsilon_T^2)}$$

where

$\varepsilon_B$ the combined errors in Bouguer gravity measurements,
$\varepsilon_g$ error in observation,
$\varepsilon_h$ error in elevation,
$\varepsilon_p$ error in position,
$\varepsilon_T$ error in terrain correction.

The errors in measurement during the regional gravity survey in the study area were found to be within $\pm 0.1$ mGal. The errors in elevation depend upon the number of benchmarks, the number of quality GPS[2] observations, topographic relief, and variability of weather. The errors in elevation $\varepsilon_h$ were calculated by multiplying the errors in elevation measurement with the combined Bouguer slab and free air correction (0.1967 mGal/m) values. The total sum of errors in the Bouguer gravity value, taking into consideration the different errors mentioned above, is $\pm 0.4$ mGal in the basin and $\pm 1$ mGal on the plateaus.

[1] 1 mGal is equivalent to 10 μm/s$^2$ (in SI-units).

[2] GPS Global Positioning System.

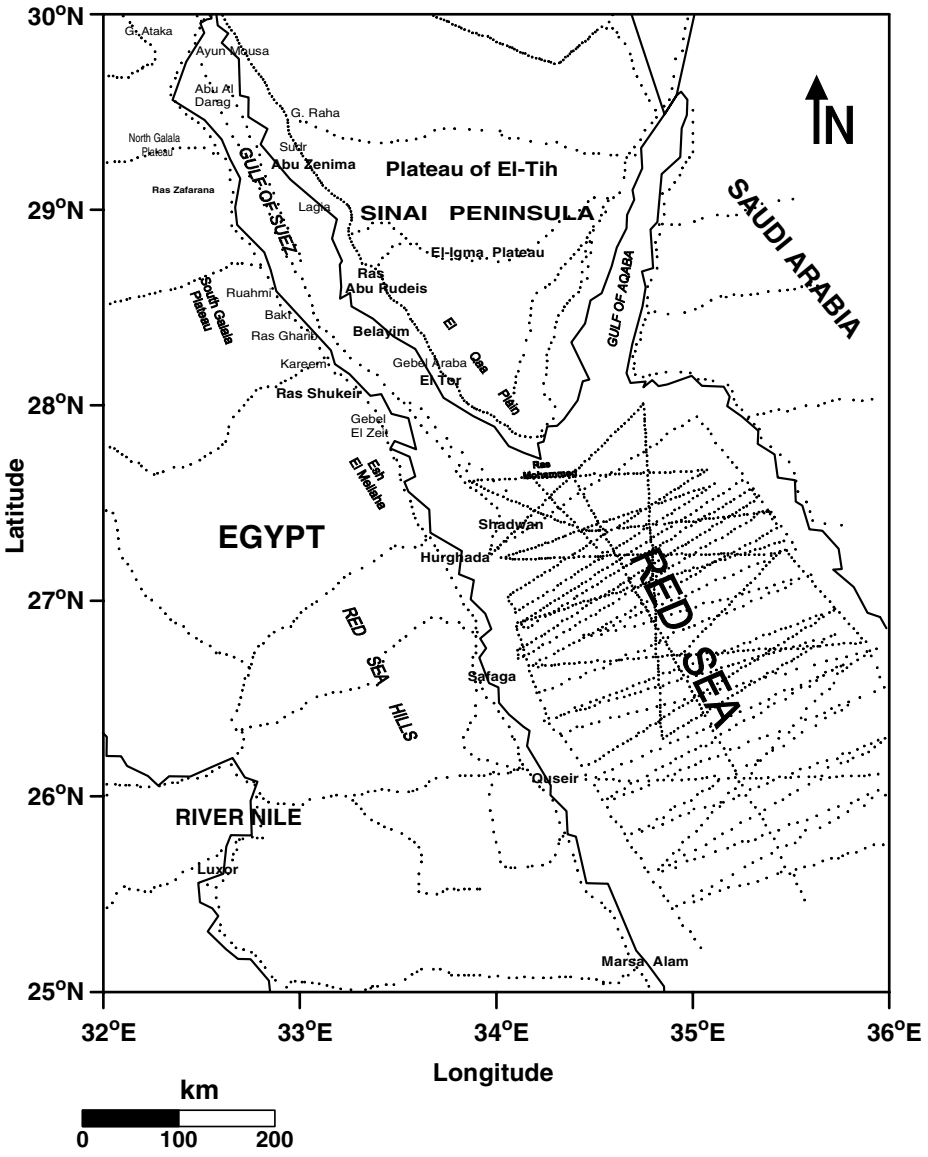


Fig. 3. Location map of the regional gravity profiles (the dots show the observation points).

In order to interpret the gross crustal structure of the northern Red Sea rift and Gulf of Suez, a new Bouguer gravity anomaly map, at a constant contour interval of 5 mGal was prepared (Fig. 4). The general trend of the Bouguer gravity anomalies is northwest–southeast. The map reveals a broad regional negative Bouguer anomaly over the entire Red Sea rift and the Gulf of Suez. The anomaly increases in magnitude with a decrease in the relief of the topography and attains its maximum of +95 mGal along the axis of the Red Sea rift floor. With the new data coverage, this map can be divided into a number of distinct areas based on anomaly size, trend and gradient, which can be related to regional geology.

A belt of first-, second- and third-order magnitude gravity anomalies extends in a northwest–southeast (Clysmic) direction in the Hurgada-Shadwan-Ras-Mohamed areas. This belt is characterised by intensive gravity variations. It may be subdivided into the following three units (comp. Figs. 2 and 4):

(1) Northern zone of the Gulf of Suez: This zone is characterised by first-order gravity anomalies both in magnitude and size. The minimum value is about −50 mGal. It is bordered by a zone of intensive gravity variation within which the local gravity high of Ayun Musa and the gravity anomaly of Suder-Lagia are located.
(2) Central zone of the Gulf of Suez: This zone is also associated with first-order gravity low anomalies of about −80 mGal. It is distinctly bordered by strips of intensive gravity variations of the meridian trend of the Zafarana, Wadi um Arta, Abu Rudeis-Belayim-Shukheir-Gharib and Lagia-Abu Zeneima areas. Within the axial part of the regional gravity

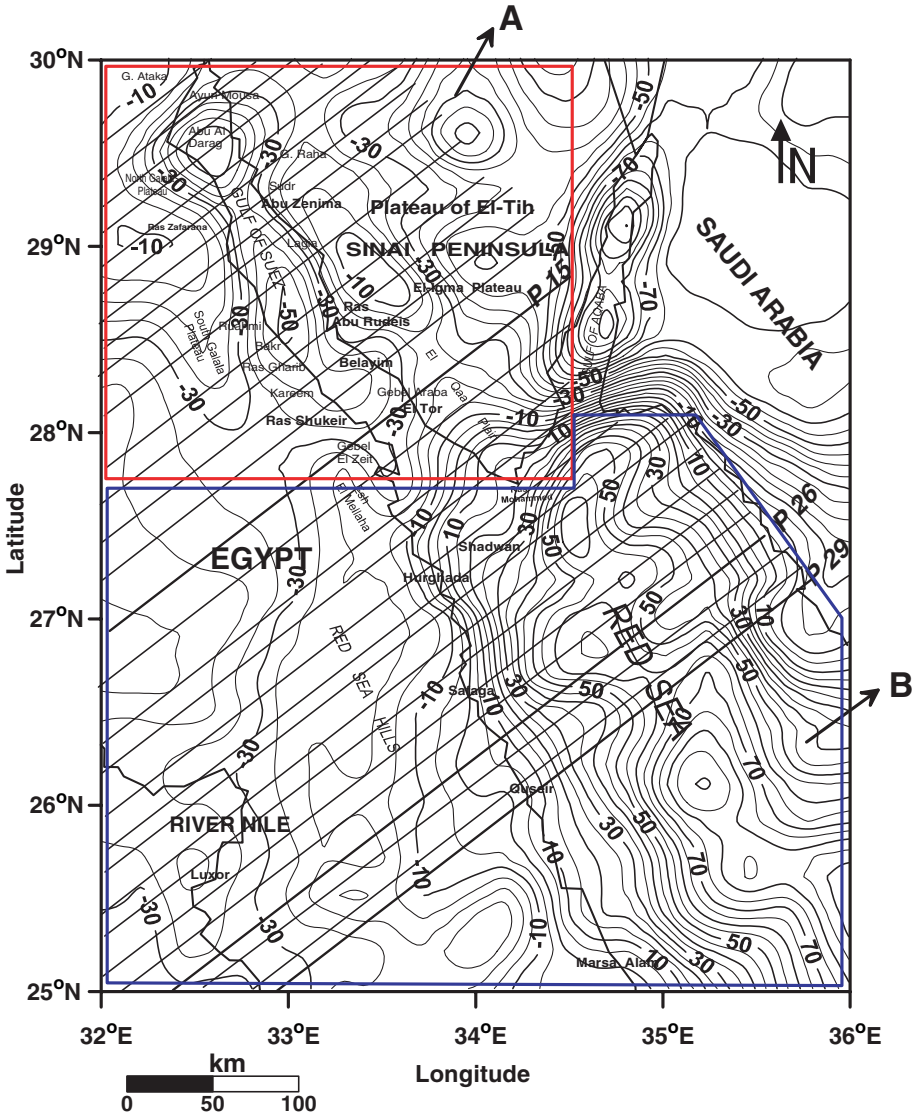


Fig. 4. Measured Bouguer anomaly map of the Red Sea and surrounding region. Contour interval is 5 mGal; gravity is reduced at Sea level. Density of reduction is 2.67 g/cm3 and the international gravity formula of 1967 has been used. The topographic reductions have been applied. This map is a simplified version of the 1:500,000 scale maps published by the GPC, Cairo, 1980.

low, local highs of clysmic trend occur at Ras Gharib, Bakr-Kareem and Gharib North. These are associated with the Kareem-west Ruahmi low which may form the Khashaba basin located to the west of Ruahmi and west Bakr.

(3) Southern zone of the Gulf of Suez: In spite of the huge data gaps, and using available profiles we can suggest that gravity anomalies in this zone are different from those of the other zones of the Gulf, in being elongated in shape. They, like all others in the area between the Gulf and the Red Sea, follow the Clysmic trend.

The first-order local low of Abu Rudeis-El-Tor lies in the Abu Durba area between Gebel Araba and the El-Qaa plain. The minimum values are − 50 mGal. A local high in the vicinity of Abu Durba is noticed in the Gebel Araba ridge. On the western side of the Gulf lies the Gebel Zeit local high which is followed to the west by a pronounced gravity low of about −40 mGal. This low may be attributed to the thick salt section of the subsurface Miocene in this part of the study area (Kamel, 1990). Further to the south, at Esh El-Mellaha range, a local gravity high of 5 mGal is observed. East of this positive gravity anomaly (Fig. 4), there is a gravity low with a value of −40 mGal. In the Galala plateau (elevation of 600 m) in the Eastern Desert, where Eocene Limestone rocks crop out, Bouguer values range from −10 to −50 mGal.

The most diagnostic feature of the composite map is a linear positive anomaly (+80 mGal) centered over the Red Sea, flanked by two small anomalies over the Arabian shield (down to +10 mGal) and over the Nubian Shield (down to −40 mGal). The total width of the anomalous zone is of an order of 300 km. The large amplitude wave

length anomalies suggest crustal inhomogeneties. It is obvious that such large-amplitude, long-wavelength anomalies cannot be produced solely by crustal inhomogeneities, and a subtantial contribution from subcrustal density variations (asthenosphere) is inferred.

The positive axial anomaly attains its maximum value of about 90 mGal in the southern part of the area. A slight systematic decrease of the amplitude occurs to the north, where the maximum amplitude is of the order 80 mGal south the entrance to Gulf of Aqaba.

The highest mountains in the Red Sea Ranges are over 1000 m, and their negative Bouguer anomalies are only about −10 to −30 mGal, aligned parallel to the Red Sea along a NNW trend. To the west of these anomalies, from 26 to 28.5 N and 31.5 to 33 E, an elongated gravity minimum with values between −35 and −50 mGal marks the Galala Basin, where almost 5 km thick sediments are limited to the east by the outcroping crystalline basement (Makris and Kebeasy, 1982). The elevation of this area is fairly smooth and only 200–400 m above sea level. The Red Sea Mountains, with altitudes over 800 m, show Bouguer anomalies between −10 mGal and −35 mGal, the values increasing to zero gravity level at the Red Sea coast. These anomalies suggest that the crust attains its maximum thickness below the Red Sea Mountains and thins considerably towards the Red Sea rift. In the Red Sea, the anomalies are positive, the anomaly increases in magnitude with a decrease in the relief of the topography and attains its maximum of +80 mGal along the axis of the Red Sea rift floor.

In eastern Egypt and the Gulf of Suez, the anomalies have a NNW–SSE trend which is associated with the Miocene and Post Miocene opening of the Red Sea and Gulf of Suez.

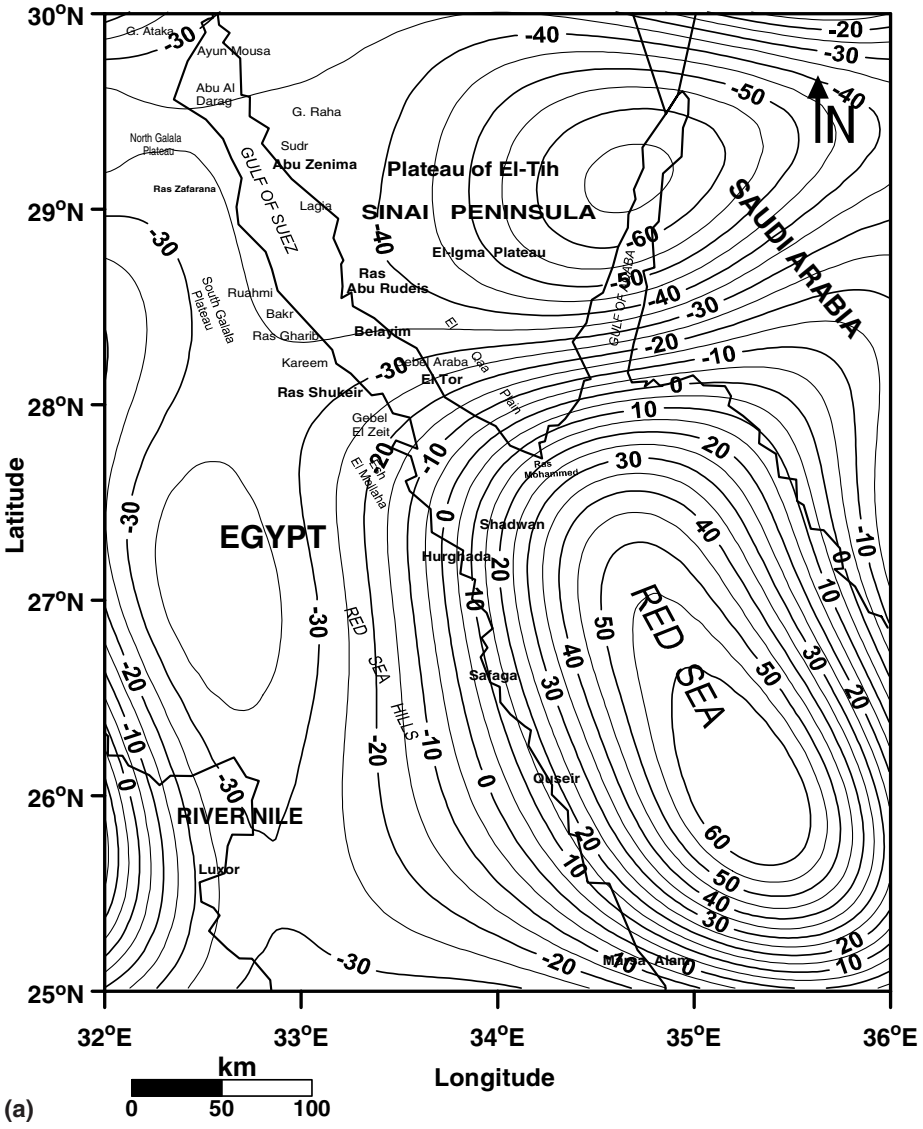


Fig. 5. (a) Regional anomaly map with an effective cut-off wavelength of 120 km and (b) residual anomaly map with an effective cut-off wavelength of 120 km.

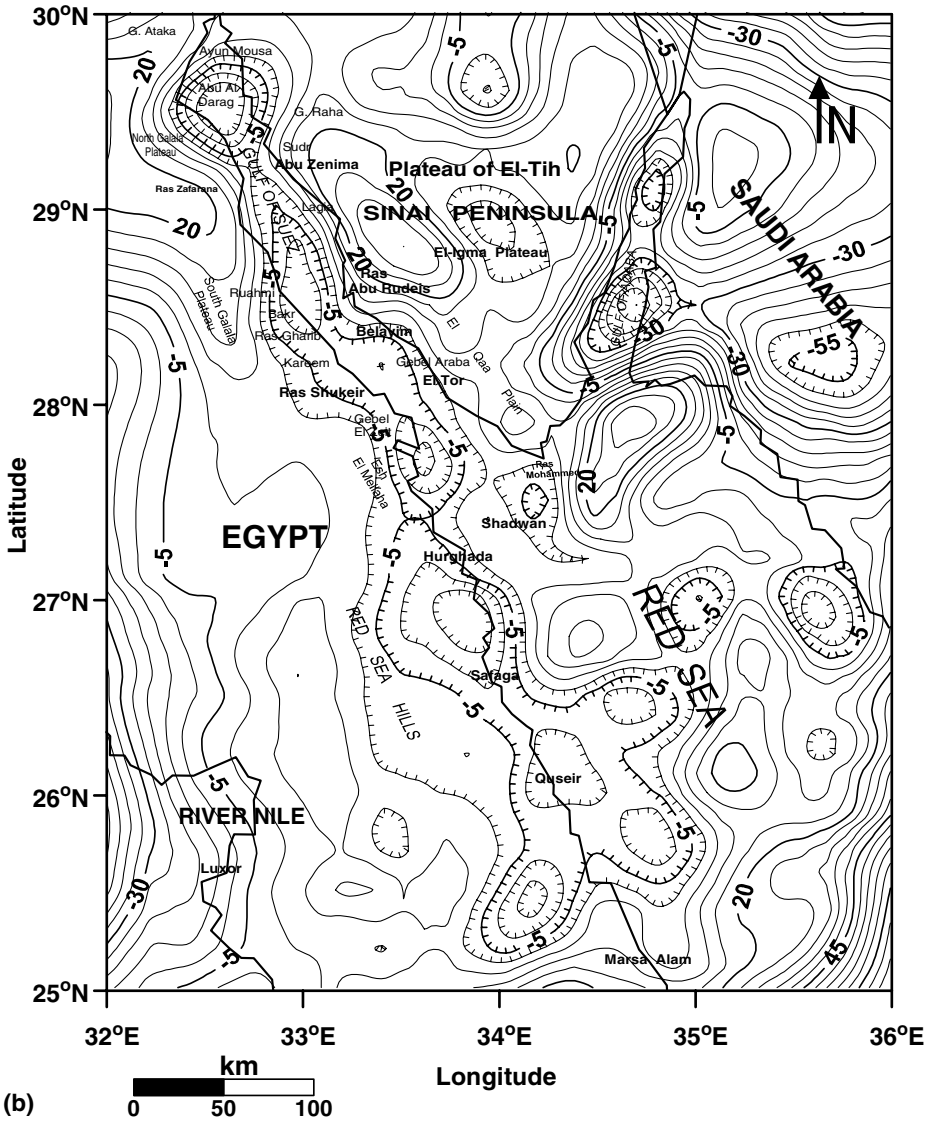


Fig. 5 (*continued*)

### 3.2. Filtering

For the purpose of detailed qualitative interpretation of the gravity anomalies, wavelength filtering was applied. This was done using FFT approach (Degro, 1986). One of the main objectives of the wavelength filtering was to attempt to relate the two main regional negative and positive anomalies to their depth of origin, and to identify persistent trends at various wavelengths of cut-off. The origin depths of the anomalies were estimated by using the 3-D approximation relationship between the maximum depth of a causative body ($Z_s$) and a certain cut-off wavelength ($\lambda_c$) given by Jung (1961) as:

$$\lambda_c \geqslant 3Z_s.$$

A total of 2400 gravity data points were filtered at different cut-off wavelengths to obtain regional anomaly maps.

The effective cutoff wavelengths were selected such that the depths of the mass centers of the causative bodies were in accordance with the results of 2-D gravity modeling; several layers could be defined.

The regional anomaly map shown in Fig. 5a is a case with an effective cut-off wavelength of 120 km, with a depth of origin of approximately 40 km. The main feature of this map is the NNW-SSE trend, where the gravity anomalies increase towards the Red Sea axial rift (eastern side) in the study area. In the Red Sea area the anomaly values increase from −30 mGal (below the Red Sea mountains) to −5 mGal at the Red Sea coast. The elliptical negative anomaly below the Sinai region, with a E–W trend, indicates clearly the increase of the crustal thickness below the Sinai region. On the other hand, in the Red Sea axial depression, the maximum value is +60 mGal due to a decrease in crustal thickness beneath the Red Sea. The

residual field map is very similar to the unfiltered Bouguer map, as shown in Fig. 5b; in addition some isolated negative anomalies can be seen along the Red Sea coast, having a NW-SE trend and values of more than −10 mGal. Similar features have been obtaind with different effective cut-off (64, 36, and 21.3 km) wavelengths.

At a cut-off wavelength of 12.8 km (Fig. 6a) the major regional trends become less clearly defined as they are now superimposed on each other. Small anomalies become clearly defined and nearly all the anomalies of the Bouguer map are represented. The sources are sedimentary layers at fairly shallow depths of approximately 4 km. The local anomaly structures are absent at this shallow depth (Fig. 6b), where there is no local structure to be recognized.

In general, due to the data gaps and the distribution of the gravity profiles we can interpret long wavelength structures, but no short wavelength information. In general, the results of the filtering operations show that the regional trend of the two main positive and negative anomalies persists between the cut-off wavelengths of 120 km and 36 km, indicating that these anomalies are probably related to regional deep-seated structures (upper mantle and or deeper crust) extending from approximately 12 km to a relative depth of 40 km.

Filtering operations at cut-off wavelengths of 21.3 and 12.8 km were conducted on the data to try and isolate superimposed effects, especially in the Gulf of Suez area. It was possible to eliminate short wavelength anomalies which are probably related to sedimentary layers at depths lower than 7 km. This trend agrees well with the geological data interpretation and the seismic refraction data (Said, 1962; Bayoumi, 1983; Makris and Ginzburg, 1987). Regarding the short wave anomalies we have to be careful in areas where we do not have data. In addition to the

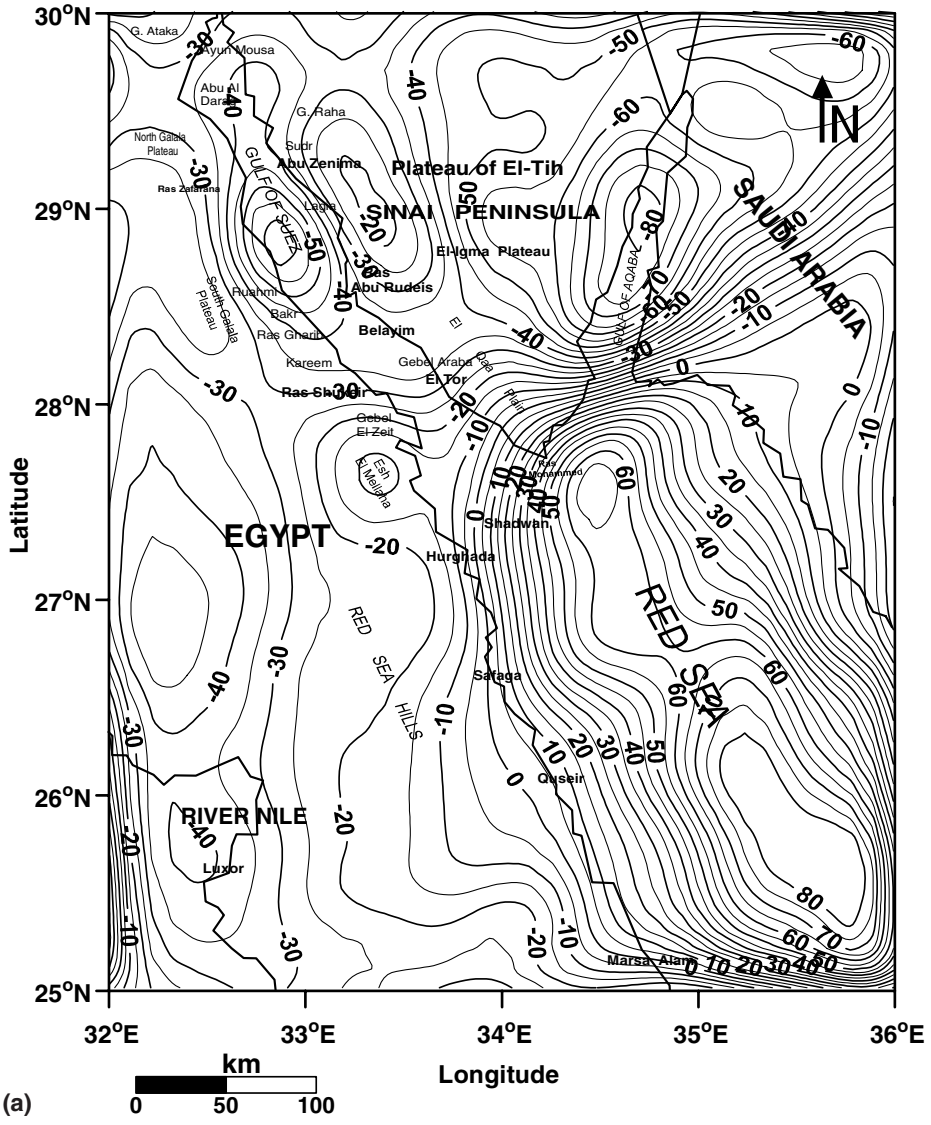


Fig. 6. (a) Regional anomaly map with an effective cut-off wavelength of 12.8 km and (b) residual anomaly map with an effective cut-off wavelength of 12.8 km.

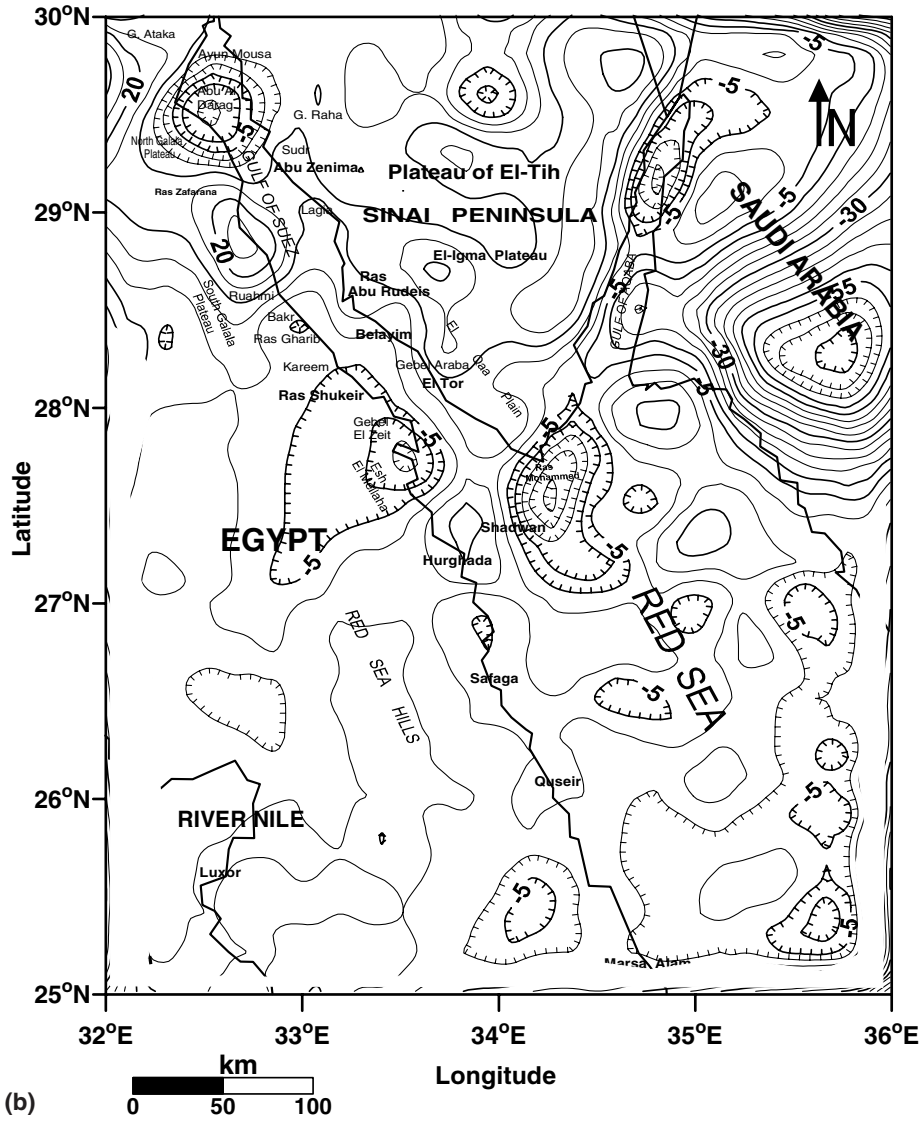


Fig. 6 (*continued*)

Table 1
The P-wave velocities of the geological units from the Red Sea region (after Gaulier et al., 1988; Marsouk, 1988)

| No. | Geological units | Description | Velocity vp (km/s) | Density kg/m$^3$ |
|---|---|---|---|---|
| 1 | Recent sediments | Undivided Quaternary and Pliocene sediments | 2.0 | 2220 |
| 2 | Evaporitic series | Eocene calcareous formation, Senomanian marls and limestones, and would correspond to Cenomanian shales and Nubian sandstones | 4.1 | 2390 |
| 3 | Igneous crust | Crust mixed materials | 5.6 | 2850 |
| 4 | Anomalous upper Mantle | – | 7.5 | 3100 |
| 5 | Miocene | Thick section of gypsum and anhydrite with marly interbeds | 4.2 | 2400 |
| 6 | Upper crust (basement rocks) | Grained quartz diorite and hornblende-biotite | 6.0 | 2750 |
| 7 | Lower crust | | 6.4 | 2900 |
| 8 | Normal upper Mantle | – | 8.0 | 3250 |

The different rock units used in the 3-dimensional gravity modeling and their respective densities.

separation of the Bouguer anomaly into its regional and residual constituents, an indirect method of interpretation (3-D forward modeling) was applied to interpret the geological structure of the subsurface.

To understand the results of this method, a short description of the theoretical background is given below.

### 3.3. Three-dimensional gravity modeling

The 3-dimensional forward gravity modeling package IGMAS (Interactive Gravity and Magnetic Analyzing System), developed by Schmidt and Götze (1998), was used to establish the geometry and density distribution of the rift. The method is based mainly on transforming the volume integral involved in the vertical attraction of a homogeneous polyhedron into a sum of line integrals suitable for computer programming. The program requires an input data structure along a definite number of vertical modeling

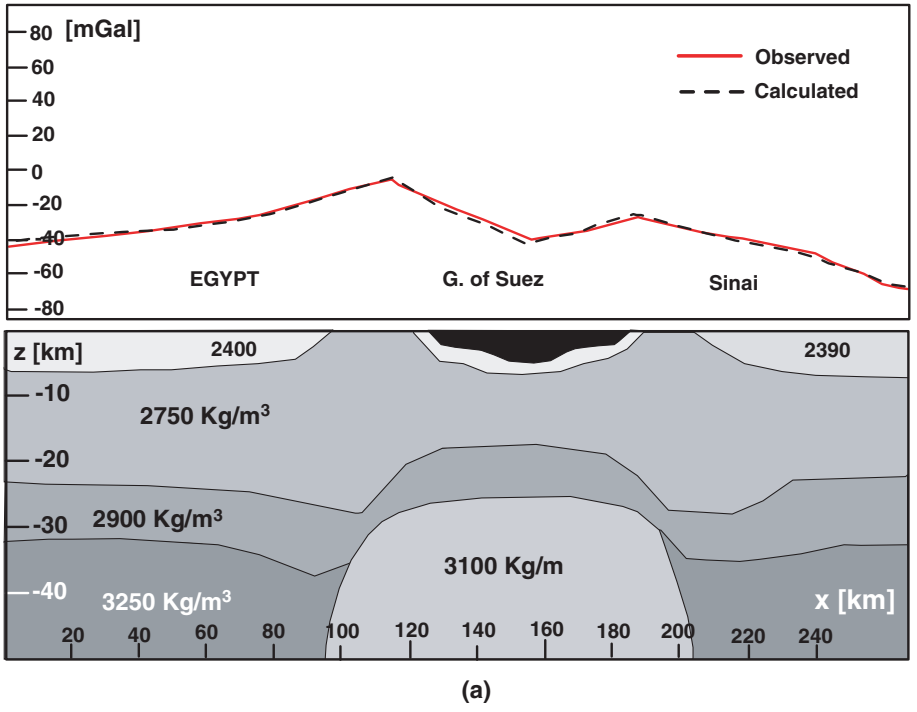


(a)

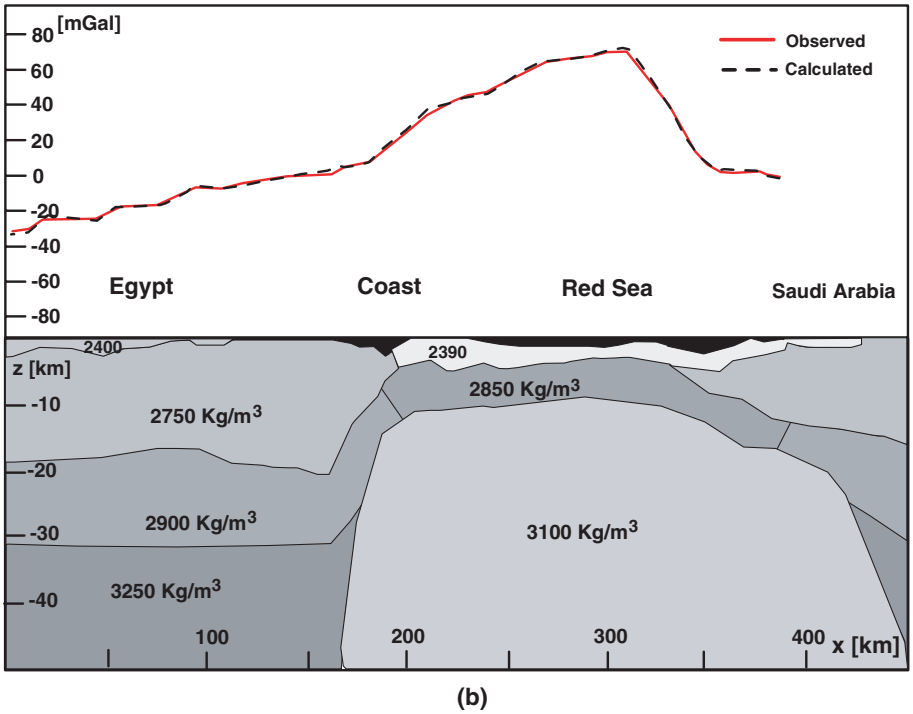


(b)

Fig. 7. (a) The vertical cross-section of the 3-D gravity model from the central sector of the Red Sea region, along plane 15 and (b) the vertical cross-section of the 3-D gravity model from the southern sector of the Red Sea region, along plane 26.

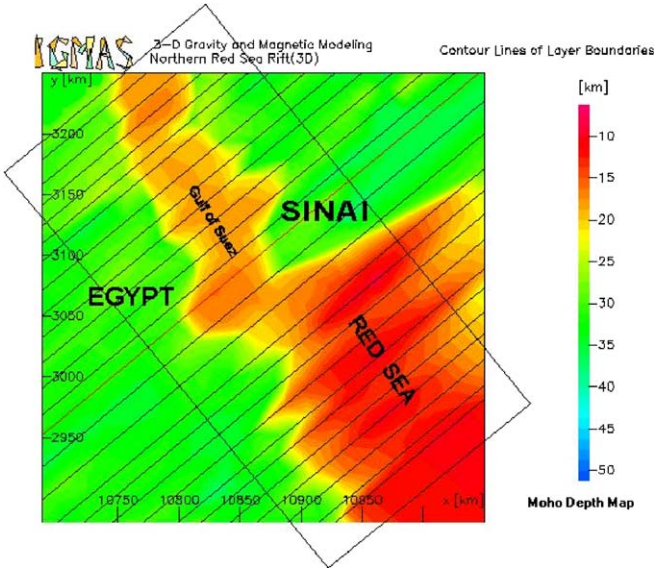


Fig. 8. Moho depth map for the area of study.

planes perpendicular to the general geological strike. In each plane, the vertices of the assumed subsurface structures are interconnected to form a line separating two media with different densities. Lines of the neighboring planes separating identical medium densities are then joined to form triangles and, hence, layer boundary surfaces. The model so developed gives a more realistic approximation of the geologic structures (Götze, 1976, 1984; Götze and Lahmeyer, 1988). One of the advantages of this method is its ability to approximate a body with a small number of polyhedrons. Consequently, any change in the shape of the body can be achieved with only a few data manipulations. Besides the simplicity of approximation in data handling and manipulation pertaining to the changes of shape of the body, the method takes care of the Earth curvature during the computation of the effects of very large structures. The results of the gravity model studies of the deep structure of the Alpine area, Harz mountains and Main Ethiopian rift are amongst the best case histories (among others) that show the applicability and effectiveness of the method (Götze, 1984; Pfister,

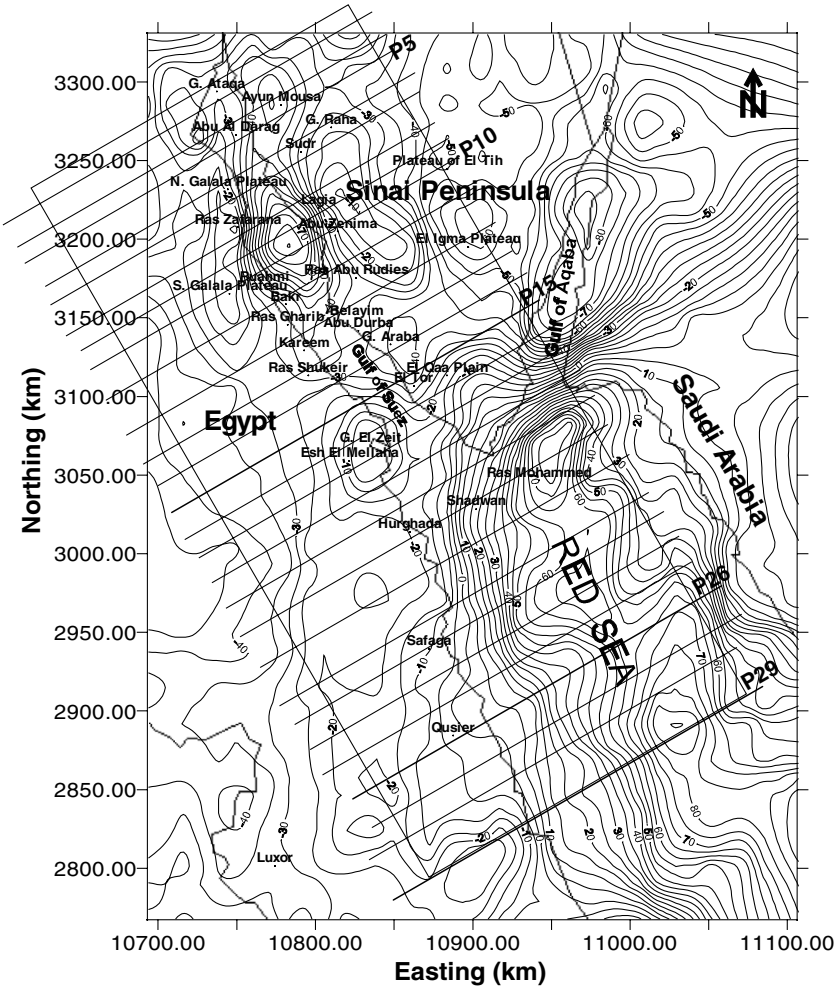


Fig. 9. Modeled Bouguer gravity map. The thin lines P2-P29 denote the locations of the gravity modeling planes 2-29. The profiles P10, P15 and P26 (bold) are explained in Fig. 8a–c. Contour interval is 5 mGal.

1988; Gabriel et al., 1996, 1997; Mahatsente et al., 1999; Jentzsch et al., 2000).

As the general geological strike along the rift floor is variable, the 3-D modeling was applied, covering an area of $18 \times 10^4$ km$^2$ (300 km × 600 km). The location and orientation of the vertical modeling planes are shown in Figs. 4 and 9. The orientation of the vertical planes is perpendicular to the general geological strike of the rift. The vertical planes are parallel to each other, and the distances between the planes are variable along the rift floor depending on the location of the anomalies, on the Bouguer map, and their corresponding causative bodies, and on the geological map. The data distribution has also been taken into consideration during the selection and orientation of the modeling planes along the investigated area.

### 3.4. Results from gravity data

The necessary information required for the 3-D gravity modeling includes the density or velocity distribution in the crust and upper mantle, the strike length, and the lateral as well as the vertical extent of the causative bodies. The better this prior information, the less ambiguous will be the final gravity model. The initial model for the gross crustal structure of the Red Sea and Suez rift consists of eight bodies representing different lithological and tectonic units.

The geometry of the initial model has been adopted from the results of the 2-dimensional gravity modeling (Makris and Ginzburg, 1987) and the seismic refraction–reflection experiment surveys conducted in the investigated area (Gaulier et al., 1988).

Table 1 shows the P-wave velocities of the structural units from the Red Sea region (after Gaulier et al., 1988; Marsouk, 1988). Also shown are the estimated density values used for the 3-D gravity modeling of the Red Sea rift. The density values were estimated from the seismic velocities using the Nafe–Drake relation (Nafe and Drake, 1957). Also it depicts the different rock units used in the 3-D gravity modeling and their respective densities. The results of

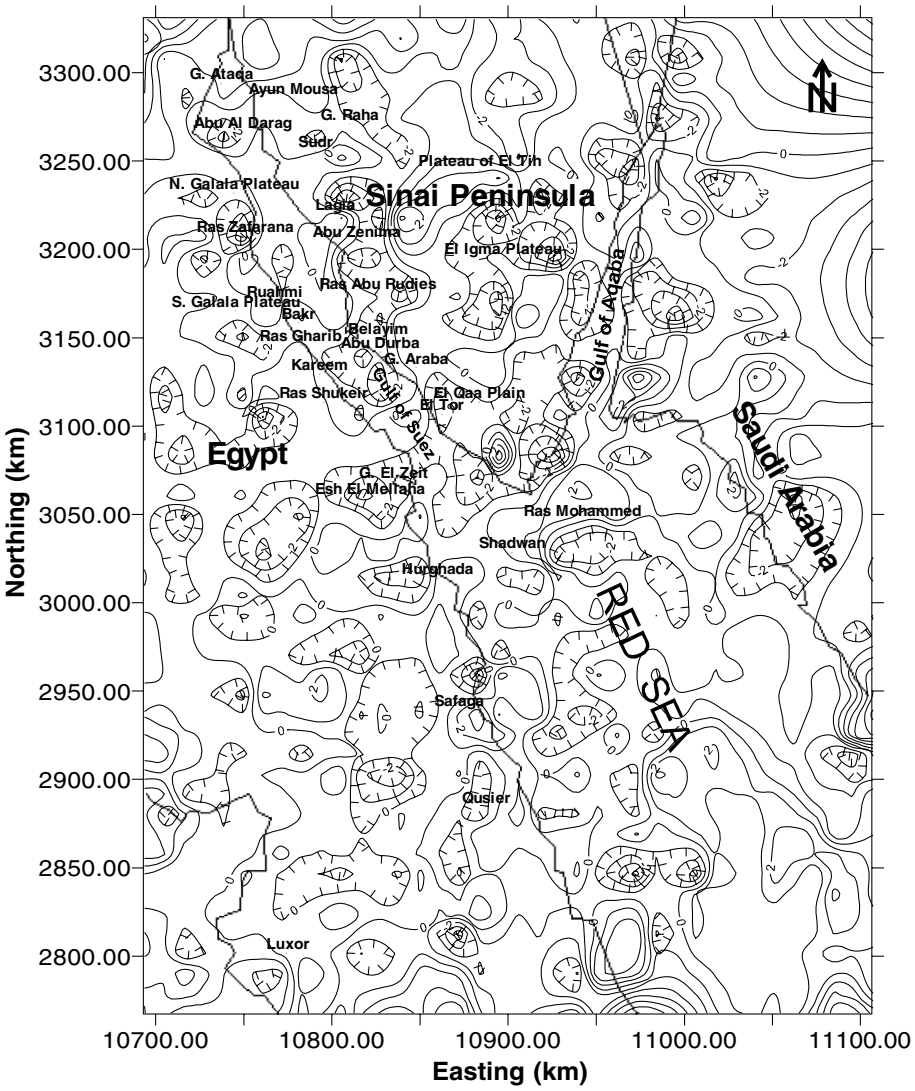


Fig. 10. The misfit between the observed and computed Bouguer anomaly of the study area. Local coordinate system is used (contour interval 1 mGal).

commercial explorations in this area (after Colleta et al., 1988; Gaulier et al., 1988; Egyptian Geological Survey, 1994) and the geological units considered in the gravity model are identified with numbers.

A section from the central sector of the Red Sea is shown in Fig. 7a (refer to Fig. 9 for the locations of the modeling planes). The long-wavelength gravity anomaly along the axial portion of the northern Red Sea rift floor is best explained in terms of a relatively low density upper mantle ($\rho = 3100$ kg/m$^3$). Its comparable seismic velocity equals 7.5 km/s, which was investigated along the axial Red Sea and Suez rifts (Gaulier et al., 1988). This anomalous layer seems to cover large parts of the main Red Sea axial rift.

This low velocity anomalous upper mantle could reflect a change in the P-T conditions (pressure release and convection heat) of the Moho, and the decrease of $v_p$ could be estimated to be −0.1 km/s (Anderson et al., 1968). This result, although it is a coarse estimation, demonstrates that the P-T parameters cannot explain the low mantle velocity of 7.5 km/s measured beneath the Gulf of Suez.

Attenuation of seismic waves with distance increases sharply from the coast to the axial area. This attenuation may be related to active fracturing and/or to higher temperatures which may indicate the presence of partial melting at depth. Hence, the previous mechanisms must be considered to explain this low velocity (the possible presence of partial melting in the upper mantle), or a pyroxenite composition for this 7.5 km/s layer, related to some underplating event (Anderson et al., 1968).

The lateral density variations in the upper mantle seem to be extremely intense in the coastal zone of the Red Sea; the low-density material is confined exclusively to the rifted area. This result is very similar to the findings of Makris and Ginzburg (1987) for the southern Red Sea as well as those of Makris et al. (1974), Berckhemer et al. (1975) in the Afar.

The gravity model also incorporates the recent sediments of the rift floor, mostly surrounded by the distribution of the basement outcrops on the Nubian side of the Gulf of Suez-Red Sea rift, as shown in Fig. 8a and b.

It should be noted that the aerial extent and degree of doming of basement crystal rocks (upper igneous crust) are far greater on both sides of the Red Sea rift than that of those bounding the Suez rift; furthermore the distribution of outcropping basement rocks is limited only to the southern half of the Gulf of Suez.

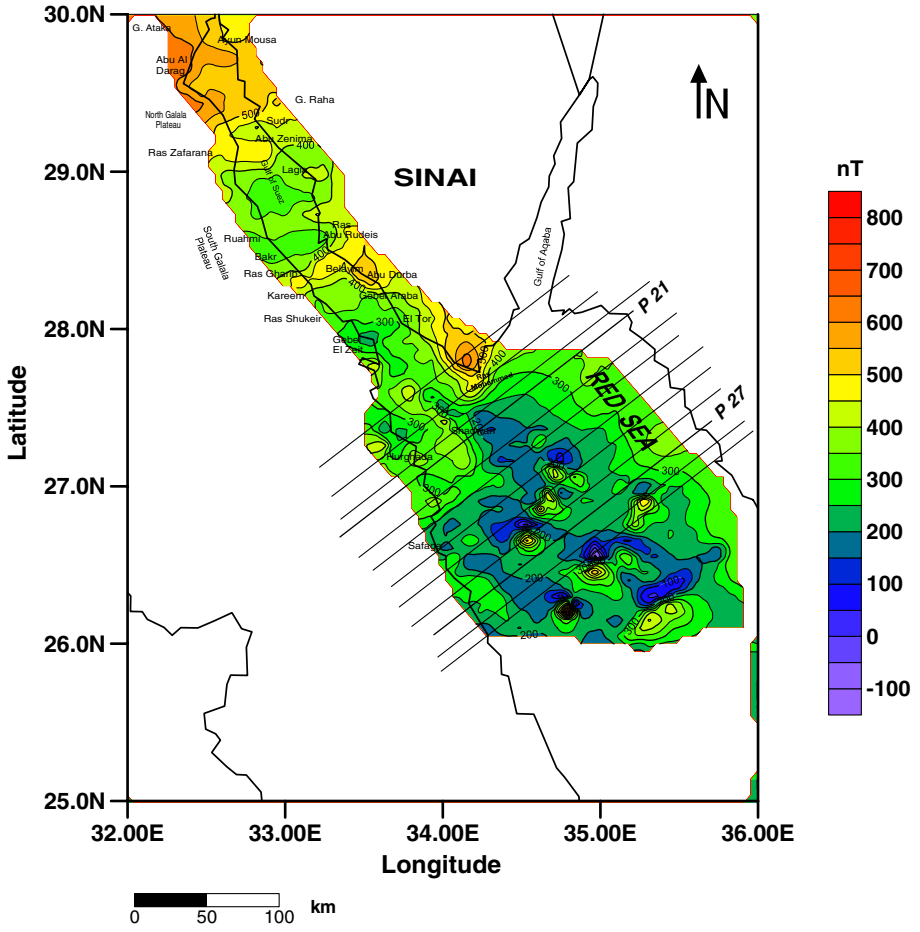


Fig. 11. Total magnetic anomaly map reduced to the pole for the studying area. Contour interval is 25 nT.

This suggests that the rate of rifting in the Red Sea is greater than that in the southern half of the Gulf of Suez, which in turn suffered more rifting than in the northern half of the Gulf. On the other hand, it is surrounded partially by evaporitic series in the northern half of the Gulf of Suez (Meshref, 1990).

As mentioned before, the negative residual anomaly is attributed to the sediments of the Suez rift. This negative residual anomaly is well explained with a density value of 2220 kg/m$^3$, 2390 kg/m$^3$ and 2400 kg/m$^3$ attached to the recent, evaporitic series and anhydrite rocks, respectively. The total thickness of the sediments in the Suez rift, as obtained from the gravity modeling, is over 7 km (Fig. 7a). The thickness of the sediment, through sparsely deposited, increases towards the central part of the Red Sea and Suez rifts (Fig. 7b).

The upper continental crust (crystalline basement), which is considered here at the bottom of the sedimentary layer was modeled with a mean density value of 2750 kg/m$^3$. Beneath the Gulf of Suez, the top interface of the crystalline basement (upper crust) is generally marked by the maximum thickness of the sedimentary layer (over 7 km, comp. Fig. 7a). The thickness of the upper crust is about 2 km under the central sector of the Suez rift. This unit generally thickens towards the adjoining plateaus (eastward to Red Sea Hills and westward to Sinai Mountains). The maximum thickness of the upper crust was found beneath both Sinai Mountains and Red Sea Hills, where the basement rocks crop out, and have a thickness of 23 km (Fig. 7b).

The lower continental crust has been modeled with a density value of 2900 kg/m$^3$. Because of the asthenospheric uplift beneath the Gulf of Suez and rifting taking place, the bottom interface of this layer with the upper mantle has a minimum depth of about 18 km.

As a result of pressure release and convection heat, indicating a more advanced stage of rifting taking place in the northern part of Red Sea rift, and being interpreted as evidence for updoming due to the sea floor spreading in the central Red Sea (Bosworth and Strecker, 1997), the crustal rocks become chiefly oceanic and consist of basalt. The model shows, that the top of this oceanic crust in the axial area of the Red Sea is relatively flat at a mean depth of 7–8 km. The minimum thickness of oceanic crust has been observed, due to the more advanced stage of rifting, to

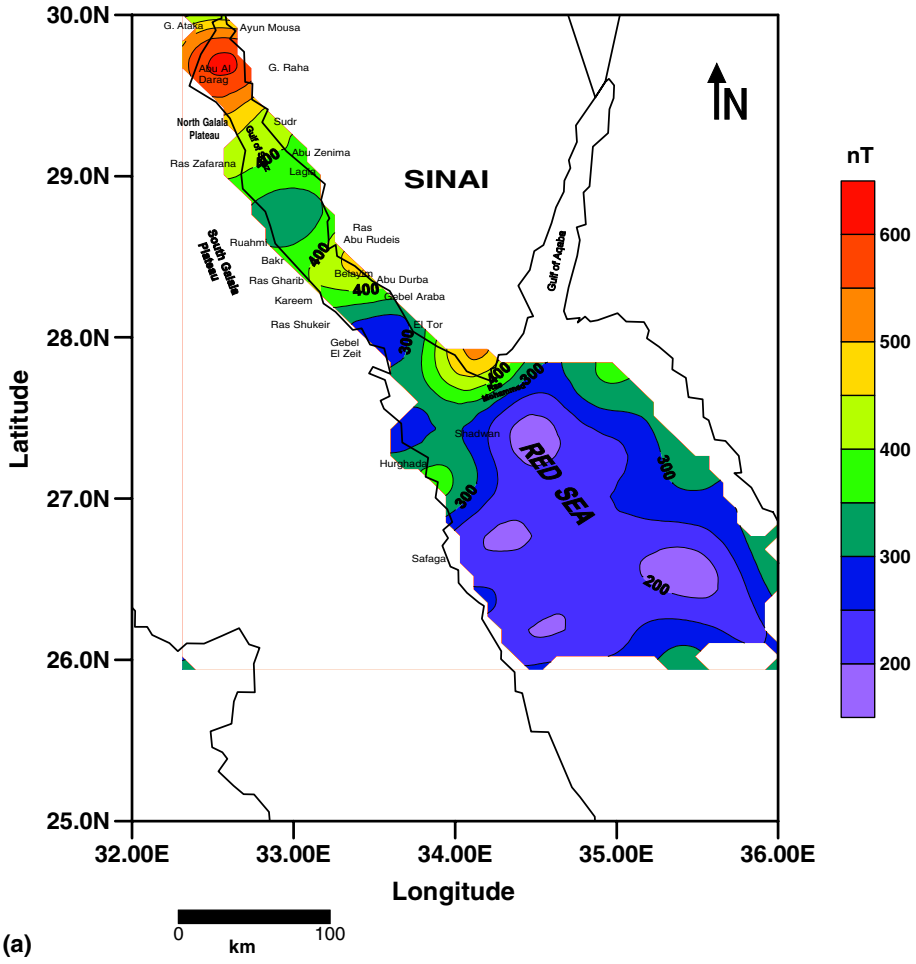


Fig. 12. (a) Regional magnetic anomaly map (of Fig. 12) with effective wavelength of 64 km. Contour interval is 25 nT and (b) residual magnetic anomaly map (of Fig. 12) with effective wavelength of 64 km. Contour interval is 25 nT.

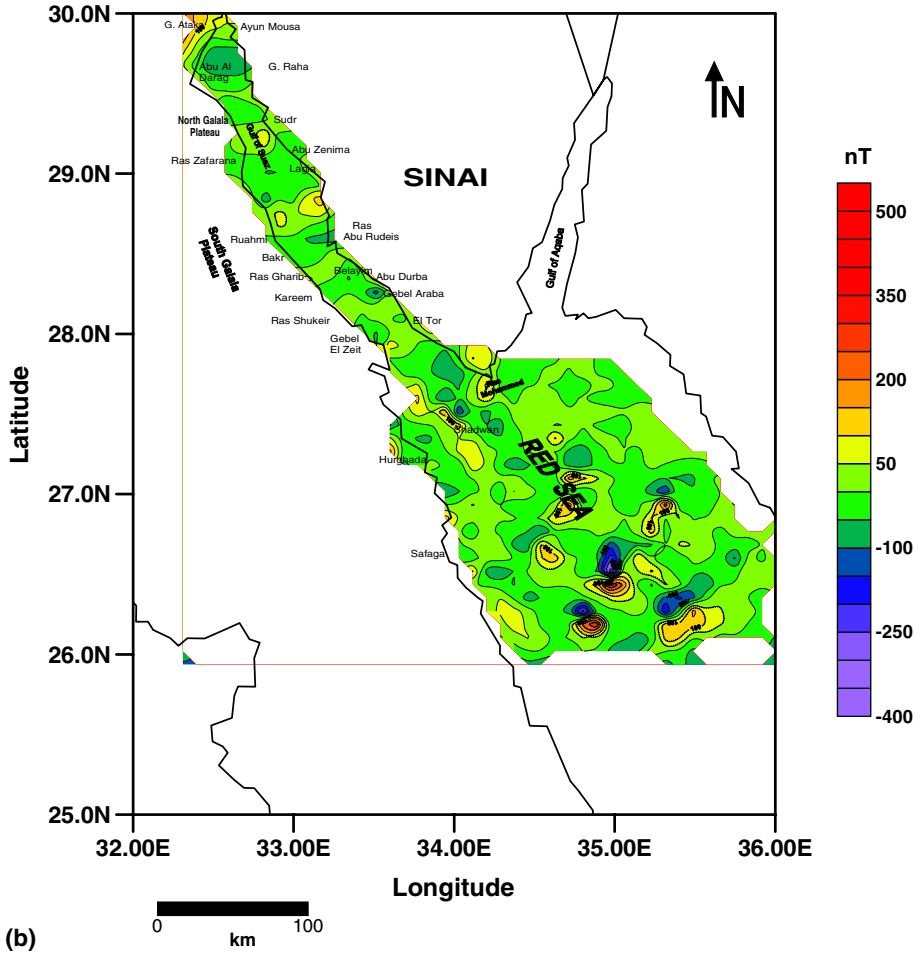


Fig. 12 (*continued*)

be 5 km (Fig. 7b). The model shows also the presence of a steep increase in crustal thickness towards the continent below the coastal plain.

The Moho depth map (Fig. 8) shows a relatively shallow depth of 18 km beneath the Gulf of Suez, and lies at a constant depth of 11–13 km at the northern Red Sea axial rift, indicating thinning of the Earth's crust in the northern Red Sea. The model also reveals a maximum Moho depth of about 37 and 35 km beneath both the Red Sea Hills and Sinai Mountains, respectively.

The first major procedure involves the fitting of the low-frequency Bouguer anomalies of the deep and large structures to the observed ones. The geometries and partly the densities of the subsurface bodies are then adjusted till the high-frequency parts of the observed Bouguer anomalies are properly modeled. The remaining discrepancies between the observed and the computed Bouguer anomalies are then further refined either by inserting new geological units into the model or with the help of the density inversion.

The latter procedure, however, needs proper constraints, because the densities obtained after inversion may or may not be realistic values. In the present study, the density values were obtained from the seismic experiment and from drilling informations of the investigation area.

In order to assess the quality of the modeling, a Bouguer map of the final model has been computed (Fig. 9). The map is ultimately in good agreement with the observed one, both in terms of the location and magnitude of the major anomalies. The centre of the gravity anomaly due to the anomalous upper oceanic mantle along the northern Red Sea rift is clearly resolved. The gravity gradients, marking the upper crust of the rift, are also well modeled. The contour map of misfit between the observed and computed Bouguer anomaly of the study area reveals an average modeling discrepancy of ±2 mGal (Fig. 10).

However, in Sinai and Gebel El Zeit, where the basement complex crops out, anomalies are prominent; the discrepancies are in the order of ±3 mGal. In such zones, it is difficult to get the best fit between the observed and the computed gravity due to small scale anomalies.

Seismically, the northern Red Sea rift is related to the northern Red Sea-Gulf of Suez–Cairo–Alexandria–Clysmic–Trend, which is considered a major active trend in Egypt. It is characterized by the occurrence of shallow, micro, small, moderate and large earthquakes. The activity

along this trend which is mainly attributed to the Red Sea rifting as well as several active faults (Kebeasy, 1990) increased in recent years.

## 4. Magnetic data

A new aeromagnetic map was compiled for both the Gulf of Suez and the northern Red Sea, based on Cochran et al. (1986), Meshref (1990). The total magnetic intensity data resulting from different aeromagnetic surveys was compiled and reduced to one set of data.

### 4.1. Magnetic data analysis

In the present work, the total intensity magnetic map of the northern Red Sea is reduced to the pole (Baranov, 1957) by using a Geosoft program 1994 (magmap Fourier domain processing system). The resulting total intensity magnetic map reduced to the pole is shown in Fig. 11. A strong regional magnetic effect, that should be subtracted from the total magnetic field in order to separate the effect of sea floor spreading, is considered to be a residual effect.

### 4.2. Filtering

For the purpose of detailed qualitative interpretation of the magnetic anomalies, wavelength filtering was applied. We follow the procedure used for filtering the graity anomalies as discussed above. But, considering the different distance relations ($1/r^2$ in gravity and $1/r^3$ in magnetic), we modified the factor in the formula of Jung (1961). Again, the depth of a causative body is $Z_s$ and the cut-off wavelength is $\lambda_c$. Then, the formula reads

$$\lambda_c \geqslant wZ_s$$

with the weight being 4.86 for a cut-off wavelength of 12.8 km, 5.77 for 21.3 km, 6.87 for 36 km, and 8.32 for 64 km, respectively. In this way reasonable depths are obtained taking into account the strong thermal gradient in the area, and thus, the shallow Curie isotherm.

The regional anomaly magnetic map shown in Fig. 12a is a case with an effective cut-off wavelength of 64 km with a depth of the origin of approximately 8 km. It shows broad and low frequency magnetic anomalies. Their values increase northward towards the Gulf of Suez. It is

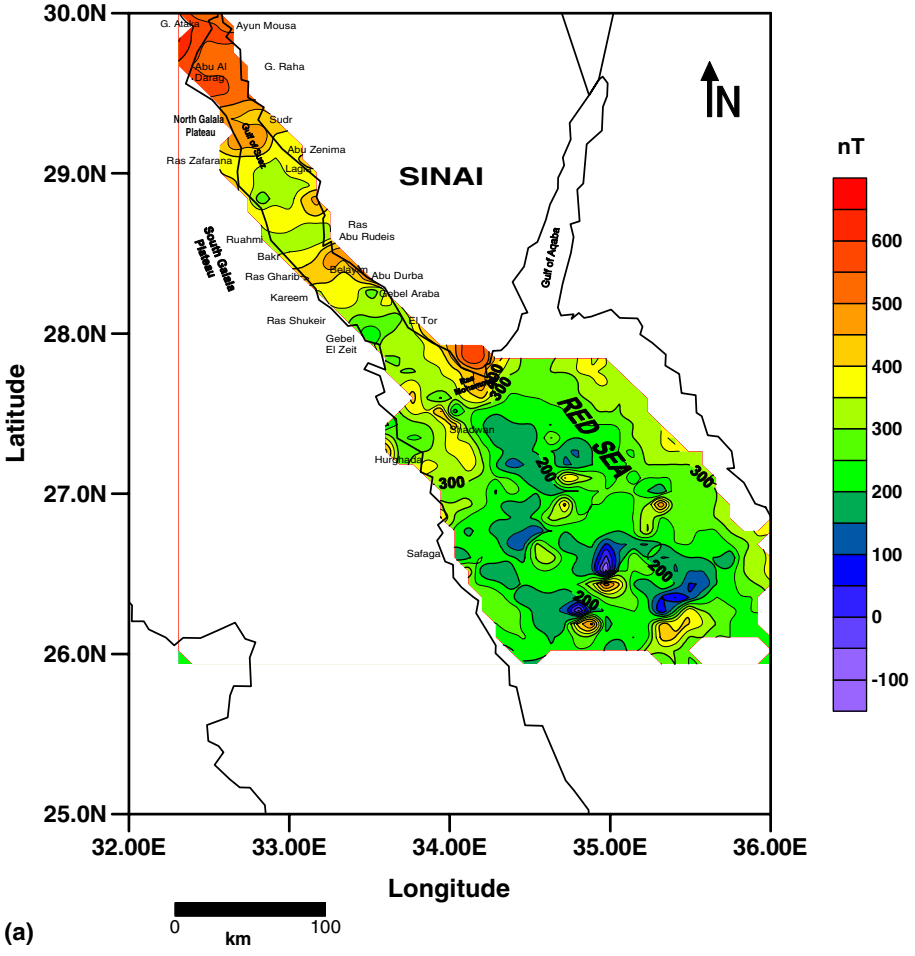


Fig. 13. (a) Regional magnetic anomaly map (of Fig. 12) with effective wavelength of 12.8 km. Contour interval is 25 nT and (b) residual magnetic anomaly map (of Fig. 12) with effective wavelength of 12.8 km. Contour interval is 25 nT.

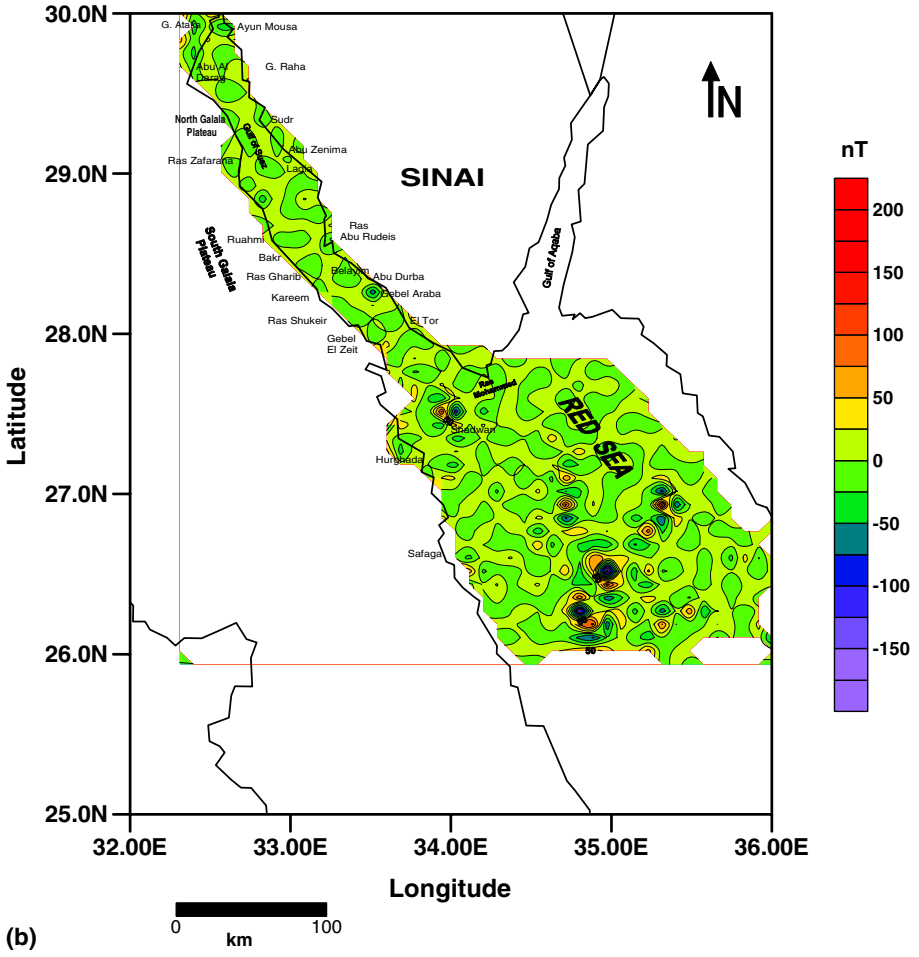


Fig. 13 (*continued*)

suggested that the main tectonic features of these deep seated structures trend northwest–southeast.

The residual magnetic map (Fig. 12b) clearly shows two main types of northwest-trending magnetic anomalies within the offshore northern Red Sea. There is a group of linear, parallel-to-coastline magnetic anomalies, of reversed polarity and of very high frequency and strong amplitude, (500–700 nT), which are discontinuous in nature and very similar to those anomalies associated with the axial trough of the central and northern Red Sea. Another group of relatively weak magnetic anomalies (50–150 nT) is distributed over the western portion of the northern Red Sea. Similar features have been obtained with different effective cut-off (36 and 21.3 km) wavelengths.

At an effective cut-off wavelength of 12.8 km (Fig. 13a), the major regional trends become less clearly defined as they are now superimposed on each other. Small local anomalies dominate and nearly all the anomalies of the Bouguer map are presented. The sources are at fairly shallow depths of approximately 4 km. The local anomaly structures are absent at this shallow depth (Fig. 13b), where no magnetic structure can be recognized.

Table 2
Magnetic susceptibilities of the geological units based on the density values of the different rock units (Schön, 1983)

| First floor | Rock type | Density kg/m$^3$ | Susceptibility mA/m |
|---|---|---|---|
| Sediment | Recent | 2000 | 13...130 |
| $Z \sim 50$ m | Sediments | 2200 | |
| Sediment | Miocene | 2450 | 2.5...13 |
| | Anhydrite | 2670 | |
| Sediment | Evaporitic series (Anhydrite) | 2390 | 2 |
| Igneous | Upper crust | 2750 | 0...1000 |
| Igneous | Oceanic crust | 2870 | 65...3800 |

### 4.3. Three-dimensional magnetic modeling

The density values were constrained as before by compressional velocities using the Nafe–Drake empirical function for the sediments (Nafe and Drake, 1957) and the Birch relationship (Birch, 1961) for the igneous crust. Magnetic susceptibilities were constrained by densities (Schön, 1983) as shown in Table 2. The region for which the 3-dimensional magnetic modeling was applied is shown in Fig. 11.

Ten vertical planes representing the tectonic distribution of the Northern Red Sea rift were modeled. The magnetic

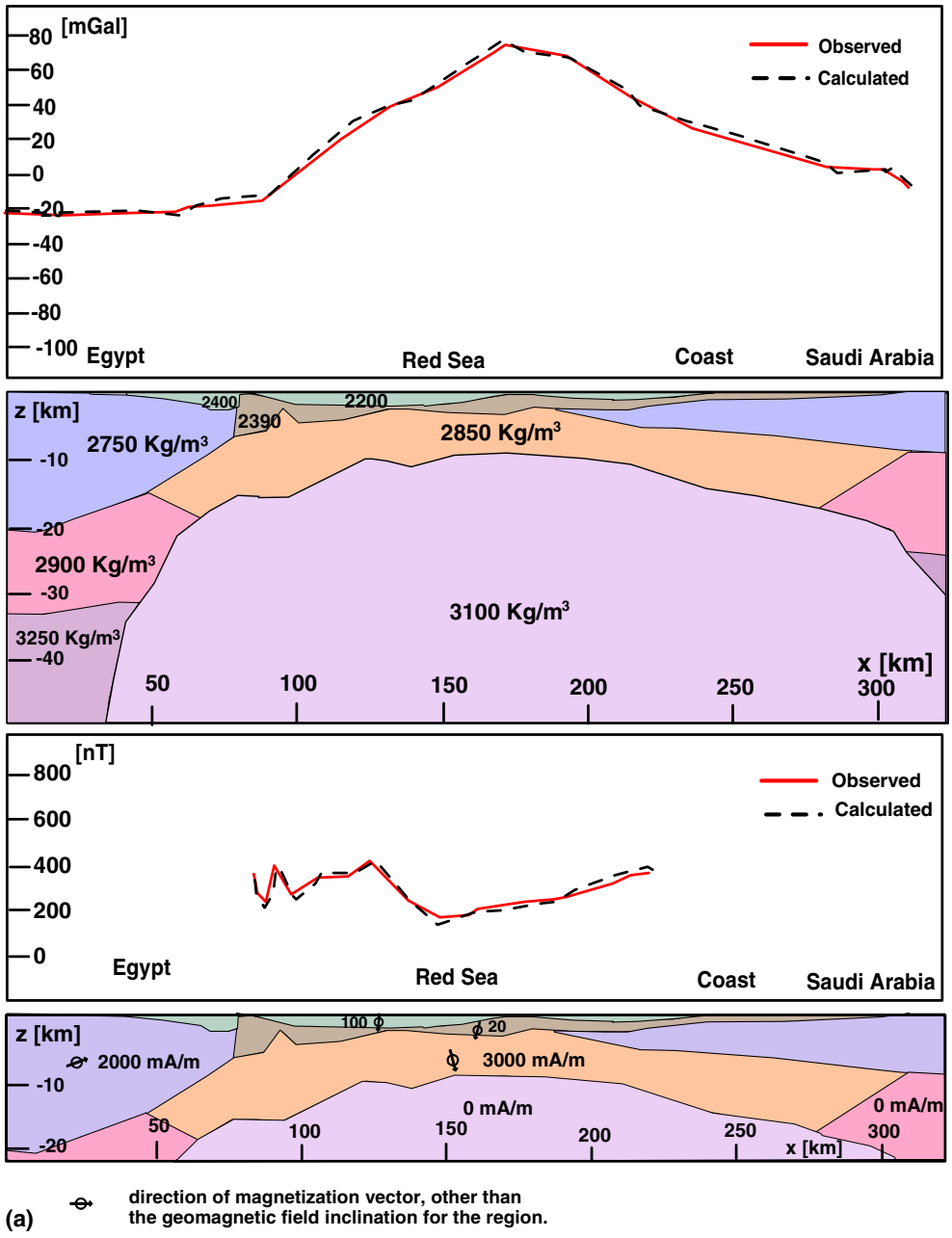


Fig. 14. (a) The vertical cross-section of the 3-dimensional gravity and magnetic model from the northern part of the main rift (plane 21) and (b) the vertical cross-section of the 3-dimensional gravity and magnetic model from the northern part of the main rift (plane 27).

profiles were selected along the same profiles as of the gravity model for the northern Red Sea.

The magnetic data will only reveal information on the part of the crust for depths with temperatures above the Curie isotherm. Rocks at higher temperatures will not show the ferromagnetic behaviour necessary to generate the discernible magnetic signal. The dominant magnetic mineral in the crust is regarded to be magnetite, which has a Curie temperature of up to 578 °C (Merrill and McElhinny, 1983). Thermal gradients of 46 °C/km and 76 °C/km are typical for continental and oceanic crust, respectively. These gradients place the Curie isotherms at depths of around 12 km and 8 km (Morgan et al., 1985; Schutz, 1994). If an oceanic-type isotherm is assumed, the magnetic data covering the Northern Red Sea region would be expected to show the topography of the oceanic crust and intra-crustal inhomogenities within the oceanic crust. As the cause for the high frequency magnetic anomaly is shallow in origin, most of the geometrical modifications done to the model were on the igneous crust and partly on the upper crust-sedimentary interface (Fig. 14a).

### 4.4. Results from magnetic data

Comparisons between simulated and measured anomalies were carried out systematically for most observed

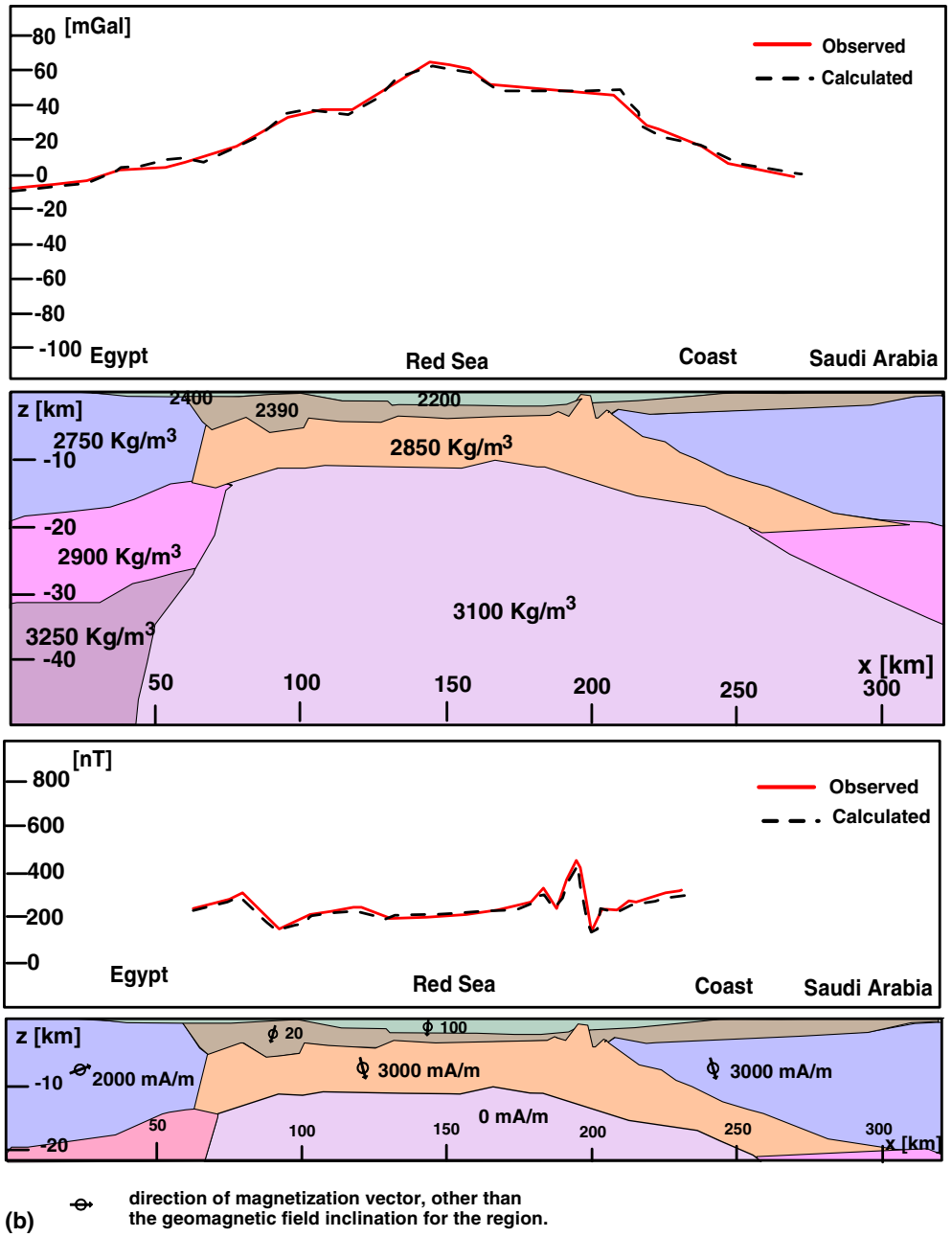


Fig. 14 (*continued*)

profiles. Exceptions were those that were believed to be distorted by transform or transverse structures or other disturbances. Excellent to good correlation exists for many profiles, which indicates that the model parameters are reasonable (Fig. 14a,b). For profiles showing good correlation between the simulated and measured profiles the maximum age and the extent of the present phase of oceanic spreading, as well as the rate of spreading of each flank are determined and compared. Spreading rates are found to decrease progressively northwards, from 0.7 cm/yr at profile 29 down to 0.5 cm/yr at profile 20. This is displayed in Fig. 15.

Seafloor spreading magnetic anomalies cannot be detected all along the axial trough of the northern part of the Red Sea. In the southern part, anomalies can be identified all along the axial trough up to profile 24. Further northward, anomalies can only be identified across short segments, being complex bipolar sets of anomalies, or very weak, hardly correlatable anomalies. In the southern part of the area, a continuous sequence of seafloor spreading anomalies can be identified on both sides of the axis, sometimes out to anomaly 2 A as far as profiles 24, 25, 27, 28, and 29.

The phenomenon of the poleward younging of continuous and discontinuous spreading ridges was recorded from the Gulf of Aden (Tisseau, 1978; Courtillot et al., 1979; Cochran, 1981) and the northern part of the Red Sea

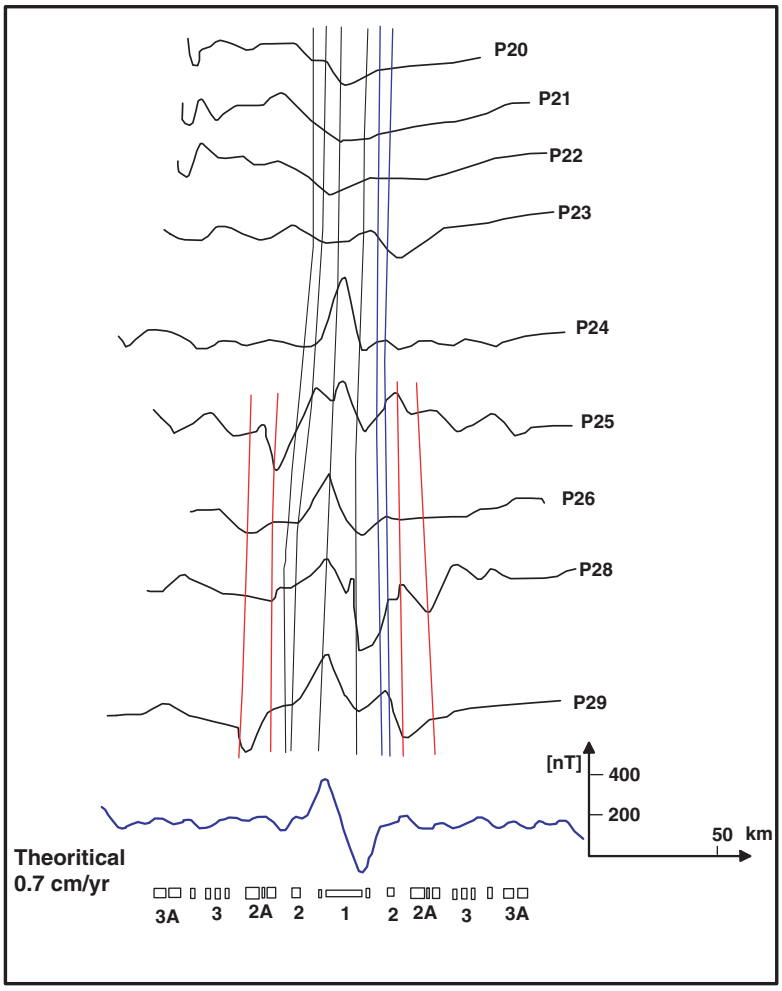


Fig. 15. Tentative seafloor spreading interpretation; the axial part of a selected number of magnetic profiles projected along the main rift. Thin vertical lines show correlation with Bonatti (1985) model. The selected profiles cover the northern part of the Red Sea from 26° to 28 °N.

(Bonatti, 1985), respectively. Courtillot et al. (1979) explained the phenomenon as the manifestation of a poleward axial propagation of a lithospheric crack. Bonatti (1985) described the phenomenon as punctiform initiation of seafloor spreading over hot areas which are related to mantle thermal waves and whose activation shows a poleward time progression. It is most probable that the Courtillot model applies to fast spreading centers (>0.7 cm/yr), whereas the Bonatti alternative applies to slow ones (<0.7 cm/yr); Hall (1979) suggested recent spreading to be 0.5 cm/yr. The magnetic anomalies over the zone beyond anomaly 3 are weak, hardly exceeding 100 nT (Fig. 15), and it can be considered to be a quiet zone. Due to magnetic contamination, seafloor spreading anomalies are not likely to be generated if spreading rates fall below a certain threshold. Rosser (1975) found that for the Red Sea this threshold is about 0.50 cm/yr.

## 5. Conclusions

Combined 3-D gravity and magnetic models which were constrained by seismic information from the Red Sea rift, Sinai Peninsula and Eastern Desert plateau, are presented in this study. The studied models reveal the existence of hot upper mantle material beneath the Red Sea rift floor. The 3-D gravity model evaluates the density distributions of the deep lithospheric structures of the Red Sea rift. The magnetic data analysis reveals the topography of the oceanic crust and intra-crustal inhomogeneties within it. Moreover, the magnetic anomalies reflect the sea floor spreading rate. The combination of gravity and magnetic data analysis has improved the geometry and the density distribution in the 3-D calculated profiles. Our results provide an important contribution towards the inferred nature and state of the crustal structure of the rift. The synthesized analysis leads to the following main conclusions:

1. On the Red Sea coast, the changes in the crust, sediment cover and upper mantle are very intense, as obtained from the 3-D gravity modeling. On the Red Sea coast the crust is still continental, only 21 km thick and at least in some areas, covered by thick sediments. The density of the upper mantle (anomalous) is very low

($\rho = 3100$ kg/m$^3$) and in agreement with the low velocities observed along the coast. A few kilometers farther to the east the nature of the crust changes completely. We find an oceanic crustal thickness that ranges from 8 to 12 km (without the thick sediments) which seems to cover large parts of the northern Red Sea rift. The distribution of the oceanic crust is not symmetric compared to the morphology of the Red Sea basin.

2. The relatively low-density of the anomalous upper mantle (3100 kg/m$^3$) of the Red Sea rift, as deduced from the gravity modeling, indicates the possible presence of partial melting in the upper mantle. The size of the area of anomalous upper mantle suggests that a large scale asthenospheric upwelling might be responsible for the subsequent rifting of the Red Sea. As a possible result of pressure release and convection heat, indicating a more advanced stage of rifting taking place in the northern part of Red Sea rift (which is interpreted as evidence for updoming due to the sea floor spreading in the central Red Sea), the crust becomes more oceanic in its nature. These results, which have been constrained by seismic measurements and confirmed by gravity and magnetic modeling, are in agreement with Cochran's concept of the northern part of the Red Sea (Cochran and Martinez, 1988).
3. The interpretation of magnetic data of the Red Sea rift shows that the spreading rate of the part south of latitude 26.5° N agrees well with the theoretical model in the order of 0.7 cm/yr. A lesser agreement is obtained in the part north of latitude 27.5 °N.
4. The Moho relief as indicated from magnetic modeling shows a poor flattening especially in the eastern region. This is contrary to what is given by other authors (e.g., Gaulier et al., 1988). However, the present results are in good agreement with the geothermal gradient values in the Red Sea (Cochran et al., 1986).
5. Finally, the lateral density variations in the upper mantle seem to be extremely intense in the coastal zone of the Red Sea, the low density material being confined exclusively to the rifted area. This result is based on Makris et al. (1988), and is very similar to the finding of Makris and Ginzburg (1987), Cochran and Martinez (1988), and by Martinez and Cochran (1988) for the northern Red Sea.

## Acknowledgements

We would like to express our gratitude to the General Petroleum Company, Cairo for utilizing the Bouguer gravity data. The authors wish to thank H.J. Götze and Sabine Schmidt for allowing us to use the 3-dimensional gravity and magnetic modeling package IGMAS. We are also indebted to the German Academic Exchange Service (DAAD) for supporting the principal author Salah S. Mohammed. This study was carried out at the Institute of Geosciences, Friedrich-Schiller-University, Jena, Germany. Also, we would like to thank M. Hussien, Institute of Petroleum Research, for encouragement and use of magnetic data.

## References

Anderson, O.L., Schreiber, E., Lieberman, R.C., Soga, N., 1968. Some elastic constant data on minerals relevant to geophysics. Rev. Geophys. 6 (4), 491–524.

Baranov, W., 1957. A new method for interpretation of aeromagnetic maps: pseudo-gravimetric anomalies. Geophysics 22, 359–383.

Bayoumi, A.J., 1983. Tectonic origin of the Gulf of Suez, Egypt, as deduced from gravity data. In: Geyer, R.A., Moore, J.R. (Eds.), Handbook of Geophysical Exploration at Sea. CRC, pp. 417–432.

Bell, R.E., Watts, A.B., 1986. Evaluation of the BGM-3 sea gravity meter system onboard R/V Conrad. Geophysics 51, 1480–1493.

Berckhemer, H., Baier B., Bartelsen H., Behle A., Burkhardt H., Gebrande H., J., Menzel H., Miller H., Vees R., 1975. Deep seismic soundings in the Afar region and on the highland of Ethiopia. In: Pilger, A., Roessler, A. (Eds.), Afar depression of Ethiopia, Stuttgart Schweizerbart.

Birch, F., 1961. The velocity of compressional waves in rocks to 10 kilobars. J. Geophys Res. 66, 2199–2224.

Bonatti, E., 1985. Punctiform initiation of seafloor spreading in the Red Sea during transition from a continental to an oceanic rift. Nature 316, 33–37.

Bosworth, W., Strecker, M., 1997. Stress field changes in the afro-arabian rift system during the Miocene to recent period. Tectonophysics 278, 47–62.

Cochran, J.R., 1981. The Gulf of Aden: structure and evolution of a young ocean basin and continental margin. J. Geophys. Res. 86, 263–288.

Cochran, J.R., Martinez, F., Steckler, M.S., Hobart, M.A., 1986. Conrad deep: a new northern Red Sea deep. Origin and implications of continental rifting. Earth. Planet Sci. Lett. 78, 18–32.

Cochran, J.R., Martinez, F., 1988. Evidence from the northern Red Sea on the transition from continental to oceanic rifting. Tectonophysics 153, 25–53.

Colleta, B., LeQuellec, P., Letouzey, J., Moretti, I., 1988. Longitudinal evolution of the Suez rift structure (Egypt). Tectonophysics 153, 221–233.

Courtillot, V., Gadeano, A., Le Mouel, J.L., 1979. Propagation of an accreting plate boundary: a discussion of new aeromagnetic data in the Gulf of Tadjourah and southern Afar. Earth Planet Sci. Lett. 47, 144–160.

Degro, T., 1986. Zur Interpretation gravimetrischer und magnetischer Feldgrößen mit Hilfe von Übertragungsfunktionen. Dissertation, Institut für Geophysik der TU Clausthal, 139 Seiten, unpublished.

Drake, C.L., Girdler, R.W., 1964. A geophysical study of the Red Sea. Geophys. J.R. Astron. Soc. 8, 473–495.

Egyptian Geological Survey, 1994. Geological map of Sinai, Arab Republic of Egypt, Scale 1:250 000.

El-Gezeery, M.V., Marsouk, I.M., 1974. Miocene rock stratigraphy of Egypt. Egypt. J. Geol. 18, 1–59.

El-Isa, Z., Mechie, J., Prodehl, C., Makris, J., Rihm, P., 1987. A crustal structure study of Jordan derived from seismic refraction data. Tectonophysics 138, 235–253.

Gabriel, G., Jahr, T., Jentzsch, G., Melzer, J., 1996. The Harz mountains, Germany: finite element modeling of the evolution based on interpretation of the gravity field. Phys. Chem. Earth 21 (4), 305–311.

Gabriel, G., Jahr, T., Jentzsch, G., Melzer, J., 1997. Deep structure and evolution of the Harz mountains: results of the three-dimensional gravity and finite-element modeling. Tectonophysics 270, 279–299.

Gaulier, J.M., Le Pichon, X., Lyberis, N., Avedik, F., Geli, L., Moretti, I., Deschamps, A., Salah, Hafez, 1988. Seismic study of the crust of the northern Red Sea and Gulf of Suez. Tectonophysics 153, 55–88.

General Petroleum Corporation, A.S.R.T., 1980. Bouguer gravity map of Egypt. Scale 1:500,000.

General Petroleum Corporation, 1986. Activity of oil exploration, Egypt, the Eighth Exploration Conference.

Gettings, M.E., Blank Jr., H.R., Mooney, W.D., Healy, J.H., 1986. Crustal structure of southwestern Saudi Arabia. J. Geophys. Res. 91 (B6), 6491–6512.

Ginzburg, A., Makris, J., Fuchs, K., Prodehl, C., 1981. The structure of the crust and upper mantle in the Dead Sea rift. Tectonophysics 80, 109–119.

Götze, H.J., 1976. Ein numerisches Verfahren zur Bereschnung der gravimetrischen und magnetischen Feldgrößen für dreidimensionale Moedellkörper. Dissertation, T.U. Clausthal.

Götze, H.J., 1984. Über den Einsatz interaktiver Comutergrafik in Rahmen 3-dimensionaler Interpretationstechniken in Gravimetrie und Magnetik. Habiltationsschrift, TU Clausthal, 236pp.

Götze, H.J., Lahmeyer, B., 1988. Application of 3-D interactive modeling in gravity and magnetics. Geophysics 53, 1096–1108.

Hall, S.A., 1979. A total intensity aeromagnetic map of the Red Sea and ist interpretation . US Geol. Surv. Saudi Arabian project, report 275, 260pp.

Hammer, S., 1939. Terrain corrections for gravimeter stations. Geophysics 4, 184–194.

Jentzsch, G., Mahatsente, R., Jahr, T., 2000. Three dimensional inversion of gravity data from the main Ethiopian rift. Phys. Chem. Earth 25 (4), 365–373.

Jung, K., 1961. Schwerkraftverfahren in der angewandten Geophysik. Akademische Verlagsgesellschaft Geest & Portig, Leipzig, 348 Seiten.

Kamel, K., 1990. Gravity map. In: Said, R. (Ed.), The Geology of Egypt. A.A. Balkema, Rotterdam, pp. 45–50.

Kebeasy, R.M., 1990. Seismicity. In: Said, R. (Ed.), The Geology of Egypt. A.A. Balkema, Rotterdam, pp. 51–59.

Mahatsente, R., Jentzsch, G., Jahr, T., 1999. Crustal structure of the main Ethiopian rift from gravity data: 3-dimensional modeling. Tectonophysics 313, 363–382.

Makris, J., Ginzburg, A., 1987. The afar depression: transition between continental rifting and sea-floor spreading. Tectonophysics 141, 199–214.

Makris, J., Kebeasy, R., 1982. South Galala Refraction Seismic Project. Paper presented at the 6th Exploration Seminar of the Egyptian General Petroleum Corporation, Cairo.

Makris, J., Menzel H., Zimmermann, J., Gouin, P., 1974. Gravity field and crustal structure of North Ethiopia. In: A., Pilger, A., Roessler (Eds.), Afar Depression of Ethiopia, Stuttgart (Schweizerbart).

Makris, J., Allam, A., Moktar, T., Basahel, A., Dehghani, G.A., Bazari, M., 1983. Crustal structure at the northwestern region of the Arabian shield and its transition to the Red Sea. Bull. Fac. Earth Sci. K. Abdulaziz Univ. 6, 435–447.

Makris, J., Rihm, R., Allam, A., 1988. Some Geophysical aspects of the evolution and structure of the crust in Egypt. In: Greiling, S.E.-G.a. R.O. (Ed.), The Pan-African Belt of Northeast Africa and Adjacent Areas, Tectonic Evolution and Economic Aspects of a Late Proterozoic Orogen: Braunschweig, Friedr. Vieweg & Sohn, pp. 345–369.

Makris, J., Henke, C.H., Egloff, F., Akamaluk, T., 1991. The gravity field of the Red Sea and East Africa. Tectonophysics 198, 369–381.

Marsouk, I.A., 1988. Study of crustal structure of Egypt deduced from deep seismic and gravity data, Ph.D. dissertation thesis: University of Hamburg, 118pp.

Martinez, F., Cochran, J.R., 1988. Structure and tectonics of the northern Red Sea: catching a continental margin between rifting and drifting. Tectonophysics 150, 1–32.

Merrill, R.T., McElhinny, M.W., 1983. The Earth's Magnetic Field. Academic Press, London, 401pp.

Meshref, W.M., 1990. Tectonic framework. In: Said, R. (Ed.), The Geology of Egypt. A.A. Balkema, Rotterdam, pp. 113–155.

Minich, G., 1987. Gravimetrische Messungen im nordischen Roten Meer, Diplomarbeit, Institut für Geophysik, Universität Hamburg, 73 Seiten, unpublished.

Morgan, P., Boulos, F.K., Hennin, S.F., El-Sherif, A.A., El Sayed, A.A., Basta, N.Z., Melek, Y.S., 1985. Heat flow in Eastern Egypt: the thermal signature of continental breakup. J. Geodyn. 4, 107–131.

Nafe, J.E., Drake, C.L., 1957. Variations with depth in shallow and deep water marine sediments of porosity, density and the velocities of compressional and shear waves. Geophysics 22, 523–552.

Pfister, H., 1988. Bearbeitung des Schwerefeldes des Harzes mit modernen Auswerte- und Interpretationsmethoden. Dissertation, Freie Universität Berlin.

Rihm, R., Makris, J., Moller, L., 1991. Seismic survey in the northern Red Sea: asymmetric crustal structure. Tectonophysics 198, 279–295.

Rosser, H.A., 1975. A detailed magnetic survey of the southern Red Sea. J. Biochem. 13, 131–153.

Said, R., 1962. The Geology of Egypt. Elsevier Publ. Co, Amsterdam and New York.

Schmidt, S., Götze, H.J., 1998. Program Documentation IGMAS. Institut für Geologie, Geophysik und Geoinformatik der FU Berlin, unveröffentlicht. 41 Seiten.

Schön, J., 1983. Petrophysik. Ferdinand Enke Verlag, Stuttgart, 405 Seiten.

Schutz, K.I., 1994. Structure and stratigraphy of the Gulf of Suez, Egypt (abs). AAPG Bull. 81 (8), 1411.

Tealeb, A., Riad, S., 1986. Regional tectonics of Sinai Peninsula interpreted from gravity and deep seismic data. In: Proceedings Fifth Annual Meeting of Egyptian Geophysical Society, Cairo, pp. 18–49.

Tisseau, J., 1978. Etude Structurale du Golfe d'Aden et du Somalie (Ocean Indien Occidental Nord). Théses Doctoral du 3 cycle, Spècialitè gèophysique interne, Universitè de Paris-Sud.

Tramontini, C., Davies, D., 1969. A seismic refraction survey in the Red Sea. Geophys. J. R. Astron. Soc. 17, 2225–2241.